Finite Element Modelling of Ultra High Performance Fibre Reinforced Concrete Beams Exposed to Fire

By

Simwanda Lenganji

A dissertation submitted to the University of Zambia in partial fulfilment of the requirements of the degree of Masters of Engineering in Structural Engineering

THE UNIVERSITY OF ZAMBIA

LUSAKA

2021

Copyright Declaration

Declaration

I, **Simwanda Lenganji**, declares that this dissertation is entirely my own work as specified in acknowledgements and that neither the dissertation nor the original work contained therein has been submitted to this or any other institution for a higher degree.

Signature: _____ Date: _____

Supervisor's name: **Dr. Charles Kahanji**

Signature: _____ Date: _____

Certificate of Approval

This dissertation of **Simwanda Lenganji** is approved as fulfilling the requirements for the award of the **Masters of Engineering** in **Structural Engineering** at the University of Zambia.

Examiner 1: _____ Signature: _____

Examiner 2: _____ Signature: _____

Examiner 3: _____ Signature: _____

Chaiperson: _____ Signature: _____

Abstract

A number of research concerns have arisen in the concrete research community on the fire resistance of Ultra-High Performance Fibre Reinforced Concrete (UHPFRC) beams, despite their improved mechanical properties at ambient temperature. The traditional experimental approach to performance-based fire resistance estimation comes with a lot of economic and physical constraints. The recent improvements in both computational power and algorithms suggest that a numerical approach to performance-based fire resistance estimation has the capability to solve some of these challenges. By building on the principle of the finite element method, in this study, finite element models of UHPFRC beams exposed to elevated temperatures in a fire were developed in a finite element software package ABAQUS. The developed finite element models were validated against experimental results reported in a previous experimental study on UHPFRC beams which were pre-loaded under load ratios of 0.2, 0.4 and 0.6 then subjected to 60-minutes ISO 834 fire in a furnace. The finite element model predicted the thermal and mechanical responses of UHPFRC beams which were in good agreement with results reported on the experimental beams. Subsequently, the finite element models were used in a parametric study to investigate the fire resistance of UHPFRC beams under nine different load ratios (0.1-0.9) and different heating regimes, that is, the ISO 834, and the hydrocarbon temperature-time curves and fire resistance ratings were estimated at 0, 30 or 60-minutes for the beams considered. It is hoped that the proposed finite element models be used directly for performance-based fire safety design of UHPFRC beams as a cost-effective numerical tool and be employed in parametric studies to develop simple prescriptive design rules.

Keywords: *UHPFRC; Load ratio ; ISO-834 fire; Steel fibres; polypropylene fibres; performance-based fire safety design*.

Dedication

This dissertation is dedicated to my daughter **Lenganji Enala Namwanda**.

Acknowledgements

Without the following people, this dissertation would have not been possible:

- First and foremost, gratitude goes to the Almighty God for giving me the breath of life and light to decipher the principles of structural fire engineering. **Psalm 36:9**
- I would also like to thank my parents and siblings for being such a blessing to me. Their great support in my academic journey cannot be ignored.
- My great appreciation goes to my supervisor Dr. Charles Kahanji, who was not only my mentor and guide but a father during moments where I lost hope and direction. I still remain inspired by this researcher, especially, his amazing works in structural fire engineering and ultra-high performance fibre reinforced concrete. I would be too proud to forget to mention his efforts in making me realize my academic career.
- The following people played an important role in offering me accommodation during my studies: Kapata, Keith, Akabondo, Namakando, Gilbert, Mr. Kalulu and Amika Usongo.

Contents

List of Figures

List of Tables

Acronyms and abbreviations

ACI - American Concrete Institute

AFGC - Association Française de Génie Civil

ASTM - American Society for Testing and Materials

CTIF - Comité Technique International de prevention et d'extinction de Feu (International Technical Committee for the Prevention and Extinction of Fire)

FEA - Finite Element Analysis

FEM - Finite Element Method

GDP - Gross Domestic Product

HC - Hydrocarbon

HPC - High Performance Concrete

HSC - High Strength Concrete

ISO - International Standard Organisations

NSC - Normal Strength Concrete

UHPC - Ultra-High Performance Concrete

UHPFRC - Ultra-High Performance Fibre Reinforced Concrete

Chapter 1

INTRODUCTION

1.1 Background

Built infrastructure such as buildings and bridges play a very important role in the socio-economic development of a country. Most of these structures are designed to last for several decades and provide functional operations to their owners throughout their service life. However, in the past two decades most buildings and bridges have suffered from several fire and explosion accidents causing more than one million fire deaths (Brushlinsky et al., 2017) and total annual loss from global fire hazard accounts for about 1 per cent of the world GDP (CTIF, 2019). With this evidence, designing structures to withstand fire actions is pivotal to ensuring life and structural safety and ensuring economical savings, especially at the face of constrained national and corporate budgets. At the core of structural fire design is the quantification of fire resistance of structural members and this may effectively be conducted within a comprehensive and robust framework called performance-based fire safety design (Dai et al., 2015) .

Due to its non-combustible nature, low heat transfer rate and good fire resistance properties Kahanji (2016), structures which are highly likely to experience accidental fires are preferred to be designed and constructed in concrete. However, when concrete structures are subjected to elevated temperatures in a fire, the mechanical properties of concrete degrade, and concrete members lose their capacity and hence their fire resistance (Dai et al., 2015). Despite this, the concrete industry is evolving and lately, there has been development of a new technology called ultra-high-performance fibre

reinforce concrete (UHPFRC). Graybeal (2007) pointed out that, in comparison to conventional concrete, UHPFRC consumes less cement, and has favourable mechanical properties such as compressive strength, tensile strength, durability, and low-strength-to-weight ratio among others.

However, UHPFRC seems to exhibit a lower fire resistance in comparison to conventional concrete. This is due the phenomenon called spalling. When UHPFRC members are exposed to fire, the moisture in the capillary pores of UHPFRC converts to steam and the escape of steam in a highly packed material exerts significant pore pressures, resulting in explosions and loss of fragments from the member (Banerji et al., 2020). The occurrence of this phenomenon reduces the capacity of the member and the explosions may be undesirable to occupants during evacuations. Such a response of UHPFRC on exposure to elevated temperatures raises many questions about the safety of the material under those conditions.

To address some of these concerns, a number of researchers have conducted experimental studies on the fire performance of full-scale UHPFRC beams in the recent past. Among a number of researchers, two notable researchers have published significant findings on the behaviour of UHPFRC in fire. The first one is Kahanji (2016) who investigated the fire performance of UHPFRC beams subjected to the ISO 834 fire in a furnace. Kahanji (2016) reported explosive spalling of UHPFRC beams with 2% and 4% (by volume) in about 15^{th} minutes into the test. The other one is a study by Banerji et al. (2020) where they investigated the influence of spalling, load level and fire scenario on the fire resistance of UHPFRC beams. In Banerji et al. (2020)'s study, UHPFRC beams were subjected to an ASTM E119 fire in a furnace and predominant spalling in the compression zone which was attributed to the absence of tensile cracks resulting in increase in pore pressure development on these portions of the beams, was reported.

Despite novel findings in the previous two studies, an experimental approach to fire design of structures is expensive and this may make performance-based fire safety design impractical. In order to make performance-based fire safety design practical, the need for numerical tools cannot be ignored. Due to being a relatively new material, numerical models for analysing the fire resistance of UHPFRC members are very scarce,

if not unavailable. The intention of this dissertation is to present a numerical model that aids in the understanding and estimation of the fire resistance of UHPFRC beams when subjected to fire. Such a tool would be very valuable for the application of performance-based fire safety design of UHPFRC beams when they are exposed to fire scenarios and for the development of simple prescriptive design rules.

1.2 Statement of the problem

The concrete industry has seen the emergency of a new material called UHPFRC. This new technology has improved mechanical properties in comparison to concrete at ambient temperature. However, when this material is exposed to fire, its fire resistance is lower than that of conventional concrete due to the high levels of spalling experienced by UHPFRC members in fire (Kahanji, 2016; Banerji et al., 2020). The need to understand the behaviour of UHPFRC in fire has in the past decade probed many researchers to investigate its fire performance.

On the other hand, the emergence of powerful computers and software programmes is changing the face of performance-based structural fire safety design. This has been due to the possibility to build numerical models on computers on which rational fire design of structures can be performed. Being a relatively new material, numerical models for analysing the fire resistance of UHPFRC beams in fire are very limited. This aim of this dissertation is to fill this research gap by adding to the body of literature, a numerical tool for simulating the fire response of UHPFRC beams for use in performance-based structural fire safety design and parametric studies to develop prescriptive design provisions.

1.3 Objectives of the dissertation

1.3.1 Research aim

The main aim of this dissertation is to develop a numerical model for simulating the fire response of UHPFRC beams.

1.3.2 Research objectives

The objectives of this study were to:

1. Develop generalised finite element models of UHPFRC beams;
2. Validate the finite element model against experimental data reported in literature; and
3. Employ the validated finite element model in a parametric study that will investigate the fire resistance of UHPFRC beams under different heat regimes and load levels.

1.3.3 Research questions

The following are the research question of this study:

1. How do the thermal and deflection response of the FE model and the experimental beams compare?;
2. What is the fire resistance of UHPFRC beams under different load levels?; and
3. What is the fire resistance of UHPFRC beams under the ISO834 and hydrocarbon fire heating regimes?

1.4 Significance of study

The finite element models developed in this study are very valuable for the application of performance-based design of UHPFRC beams exposed to fire scenarios. The numerical models set a foundation for future studies that would focus on improving these models to account for the effects that the models developed here, do not simulate. It is also hoped that the finite element models proposed in this study would be employed in parametric studies to develop simple prescriptive design rules for use in routine practice.

1.5 Conceptual Framework

The general concepts of this study and their relationships and how they underpin the current study are discussed. Figure 1.1 depicts the relationship that exists between the various concepts underpinning this study. The general research area of this study is the performance of beams exposed to fire. In structural fire engineering, the performance of structural elements (beams in this case) exposed to fire is usually expressed in terms of fire resistance ratings.

There are two approaches that can be considered, that is, the prescriptive approach and the performance-based approach. The prescriptive approach involves following simple design rules and estimating the fire resistance of the beam based on prescribed information provided in codes of practice. The performance based approach is more robust and rational, in that the beam whose fire resistance is sought, is cast and subjected to fire testing in the furnace. The performance-based approach is highly recommended by structural fire engineers, unless, in cases where time is a limiting factor.

There are two possibilities of performing performance-based fire resistance assessment of beams, that is, experimental and numerical approaches. Experimental approach is time-consuming, expensive and sometimes too difficult to conduct, especially in cases where it is difficult to place thermocouples in certain critical regions of the beam. The versatility of modern finite element software packages can exploit the powerful capabilities of the finite element method in solving complex engineering problems and therefore, estimate the fire resistance of a beam numerically.

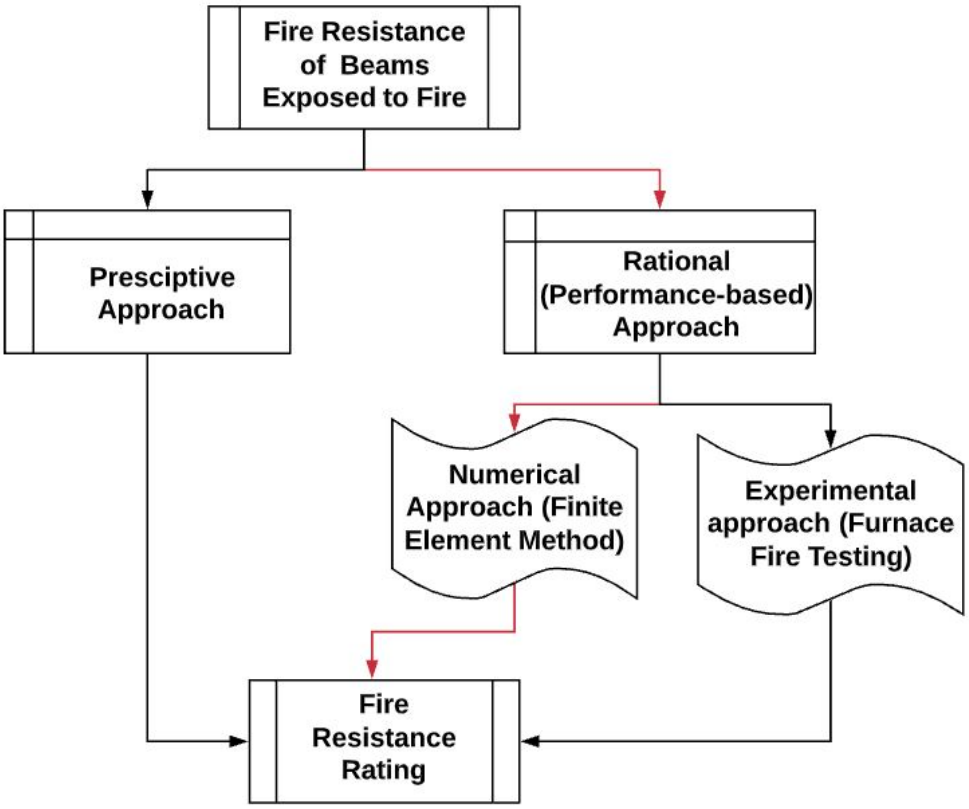

Figure 1.1: Conceptual framework of the study. Red lines indicate the path taken by the current study.

1.6 Dissertation outline

The dissertation consists of five chapters including the current introduction chapter.

Chapter 2: Literature review- This chapter starts by outlining the definitions, key characteristics, constituents, material and mechanical properties and applications of UHPFRC at ambient temperature. Then it delves into then delves into the body of the literature review and then the chapter is concluded by giving an overview of the literature reviewed while highlighting the current research gap that probed the study presented in this dissertation.

Chapter 3: Methodology- This chapter commences by highlighting that a numerical and computational approach is adopted in this dissertation, implying a positivist epistemological standpoint. Then the chapter documents experimental data obtained on UHPFRC beams as reported by Kahanji(2016) and the focus is given to the experimental setup. The methodology applied to develop the finite element models are then presented.

Chapter 4: Results and discussions- This chapter starts by presenting and discussing results obtained during the heat transfer phase of the simulation programme. The chapter then delves into presenting and discussing results obtained during the structural analysis phase of the simulation programme. A parametric study is then presented and the limitations of the model are highlighted. Lastly, an overview of the chapter is given.

Chapter 5: Conclusions and recommendations- The main conclusions drawn from this study are presented. Then the main research contribution achieved by this dissertation is highlighted. The challenges that were faced during the study are presented and then the chapter ends by giving recommendations, in terms of what can be improved and future research directions.

Chapter 2

LITERATURE REVIEW

2.1 Introduction

The advantages that come with ultra-high-performance fibre reinforced concrete (UHPFRC) has motivated many researchers and industrial experts over the past two decades to develop UHPFRC with favourable mechanical properties. Development of UHPFRC is still in progress and the need for substantial research into this material cannot be ignored. Despite notable increase in durability at ambient temperature, UHPFRC seems to have a lower fire resistance when compared to normal concrete. Development of a numerical tool to understand the fire behaviour of UHPFRC is a central component being achieved by this study. In this chapter, a review of literature on which this study is anchored, is presented and discussed.

2.2 UHPFRC at ambient temperature

2.2.1 Concrete classification

Concrete is classified into three major classes based on strength. The three classes are normal strength concrete (NSC), high performance concrete (HPC) and ultra-high-performance concrete (UHPC).

The American Concrete Institute (ACI) defines HPC as “concrete meeting spe-

cial combinations of performance and uniformity requirements that cannot always be achieved routinely using conventional constituents and normal mixing, placing, and curing practices" (American Concrete Institute, 2018) whereas (Neville, 2012) defines HPC as concrete with a compressive strength above 60MPa. Apart from having a higher compressive strength, HPC outstands NSC in terms of both performance and durability (Kahanji, 2016). The high compressive strength in HPC is achieved by adding water reducers which decrease the water to cement ratio while the compact matrix is maintained by addition of silica fume.

With compressive strength much higher than 60MPa, low water to cement ratios and high density packing result in lower porosity and HPC begins to be regarded as UHPC (Wille et al., 2011). When fibres are added to UHPC mix to improve its ductility, compressive strength, durability and toughness UHPC begins to be termed as ultra-high fibre reinforced concrete (UHPFRC).

The addition of steel fibres to the mix has shown to increase tensile strength and ductility (Park et al., 2012; Wille et al., 2014). Apart from the improved mechanical properties, UHPFRC is lighter than NSC making it favourable for high rise and bridge construction where there is a large trade-off between dead and live load capacity of the member.

2.2.2 Constituent materials

UHPFRC is basically composed of cement, fine aggregates, silica fume, metallic or hybrid fibres superplasticisers and water. Table 2.1 gives a typical mix composition of UHPFRC.

Key features that differentiate UHPFRC from NSC can be noted and these include: The low water to cement ratio as a result of addition of steel fibres; the absence of coarse aggregates; a high composition of granular materials, that is, fine sands and silica fumes which give it a more compact matrix resulting in high compressive strength; an addition of steel fibres which increases the tensile strength ; and addition of polypropylene fibres which increases its fire resistance. More information about the superplasticisers, silica fume, steel and polypropylene fibres can be found in specialised literature (Guerrini, 2000; Naaman, 2003; 2009). The melting of polypropylene fibres at high temperature

provide pore spaces for the dissipation of pore-pressure and this reduces the possibilities of spalling and hence, increasing the fire resistance of UHPFRC elements.

Table 2.1: Typical composition in UHPFRC

Constituent	composition
Cement[b]	650-967 [kg/m^3]
Watert[b]	107-190 [kg/m^3]
Cement to water ratio[a]	20%
Fine sand[c]	354-1016 [kg/m^3]
Silica fume[b]	135-275 [kg/m^3]
Superplasticiser [a]	24-35 [kg/m^3]
Quartz[c]	158-325 [kg/m^3]
Steel fibres[b]	$2\% - 2.5\%$
Polypropylene[b]	4 [kg/m^3]

a-(Habel et al., 2006), b-(Benjamin A., 2006), c-(Shi et al., 2015)

2.2.3 Applications of UHPFRC

Despite extra effort required in development of structural design provisions for UHPFRC members, several structures, especially bridges can be noted where UHPFRC has been used as a construction material. The first application was on the Sherbrooke pedestrian bridge in Quebec, Canada in 1997. Other example applications on bridges and nuclear power plants are reported in literature (AFGC, 2013; Bernardi et al., 2016).

2.2.4 UHPFRC mechanical properties at ambient temperature

2.2.4.1 Tensile strength

UHPFRC members tend to display high tensile strengths in comparison to NSC members. This property is very important as far as design of UHPFRC members for flexure is concerned. Tensile strength of UHPFRC is determined using direct and flexural tensile strength tests. Japan Society of Civil Engineers (2008) reports a mean tensile strength of 5 MPa while the AFGC (2013) report mean direct and flexural tensile strength values of 8 and 8.1 MPa as design values, respectively. Addition of steel and/or hybrid fibres can lead to tensile strength values that fall in the range 7-15 MPa (AFGC, 2013).

2.2.4.2 Compressive strength

When determining the capacity of concrete members, compressive strength is one of the most important design parameters considered. For example, it is one of the parameters required to calculate the moment of resistance of a concrete beam (EN 1992-2, 2005). Just like NSC, the compressive strength of UHPFRC is determined from either cylinder or cube compression tests and the compressive strength is a function of parameters like curing regime, materials used in the mix, water content among others (Kahanji, 2016). The characteristic compressive strength of UHPFRC ranges between 150 and 250 MPa (AFGC, 2013; Japan Society of Civil Engineers, 2008).

2.2.4.3 Elastic modulus

There are designated test methods for determining the elastic modulus of UHPFRC. However, in cases where such test tools are unavailable, an estimate of the elastic modulus can be calculated by using relationships between elastic modulus and other mechanical properties. The most common mechanical property used is characteristic compressive strength. Among other researchers, Graybeal (2007)formulated an empirical equation relating the elastic modulus for a given value of characteristic compressive strength (see Equation 2.2.1).

$$E = 3840\sqrt{f'_c} \tag{2.2.1}$$

Where E and f'_c are the elastic modulus and compressive strength of concrete, respectively.

2.2.4.4 Poisson's ratio

Poisson's ratio is a function of the constituent materials in UHPFRC. If no such a value is available, AFGC (2013) recommends a Poisson's ratio of 0.2. An experimental study by Shafiifar et al. (2017) reported a Poisson's ratio of 0.18 for UHPFRC.

2.3 UHPFRC at elevated temperatures

2.3.1 Background

Concrete, in general, due to its non-combustible nature and low rate of heat-transfer, has a good fire resistance and therefore, does not normally require any fire protection. This desirable property of concrete makes it a suitable material for compartmentalising fire in one location of the building and preventing it from spreading to neighbouring compartments of the building (Kahanji et al., 2016). Despite, this favourable property, when subjected to elevated temperatures, concrete's mechanical properties degrade leading to decreased loading capacity.

Research into the fire performance of UHPFRC is limited, though in the past decade, a number of researchers have performed experimental studies on this subject (Kahanji, 2016; Banerji et al., 2020). However, experimental approaches are time consuming and expensive, and hence the rising need for numerical tools. For such tools to be successful, understanding of thermo-mechanical behaviour of UHPFRC or concrete at elevated temperatures is imperative.

Due to limited information on the UHPFRC, some of thermo-mechanical properties presented in the this section are based on values reported in EN 1992-1-2 (2008) on normal strength concrete.

2.3.2 Mechanical Properties

2.3.2.1 Density

The density of concrete decreases with temperature. The level of moisture content in concrete which is dependent on its age also affects the density of concrete. As concrete is heated, the moisture evaporates and this leads to a reduction in density. By accounting for this moisture content, EN 1992-1-2 (2008) gives equations (see Equations 2.3.1-2.3.4) for estimating the density of concrete over a range of temperature.

For $0^oC \leq \theta \leq 115^oC$

$$\rho(\theta) = \rho(20^oC) \tag{2.3.1}$$

For $115^oC \leq \theta \leq 200^oC$

$$\rho(\theta) = \rho(20^oC) \cdot \left[1 - 0.02\left(\frac{\theta - 115}{85}\right)\right] \tag{2.3.2}$$

For $200^oC \leq \theta \leq 400^oC$

$$\rho(\theta) = \rho(20^oC) \cdot \left[0.98 - 0.03\left(\frac{\theta - 200}{200}\right)\right] \tag{2.3.3}$$

For $400^oC \leq \theta \leq 1200^oC$

$$\rho(\theta) = \rho(20^oC) \cdot \left[0.95 - 0.07\left(\frac{\theta - 400}{800}\right)\right] \tag{2.3.4}$$

Where $\rho(20^oC)$ and $\rho(\theta)$ is the density at ambient and at a given temperature, respectively.

2.3.2.2 Elastic modulus

The modulus of elasticity (E) of concrete depends on the water-cement ratio in the mixture, age of concrete, curing regime and the nature of the aggregates. With rise in temperatures, the elastic modulus reduces rapidly and the fractional decline does not significantly depend on the aggregate type (Bahr et al., 2013). A number of studies on NSC and HPC have reported the evolutions of elastic modulus with temperature. Figure 2.1 shows the evolution of elastic modulus with temperature as reported in literature (EN 1992-1-2, 2008; Phan, 1996; Castillo and Durrani, 1990).

2.3.2.3 Compressive strength

The compressive strength of concrete also decreases with increase in temperature. The temperature dependent compressive strength is a function of the curing regime. In production of UHPFRC, two curing regimes are usually considered, that is, cold curing and hot curing. The former is cured at ambient temperature and the latter is cured at 90^0C. Kahanji et al. (2018) investigated how the compressive strength of cold and hot-cured UHPFRC decreases with temperature. The relative residual compressive

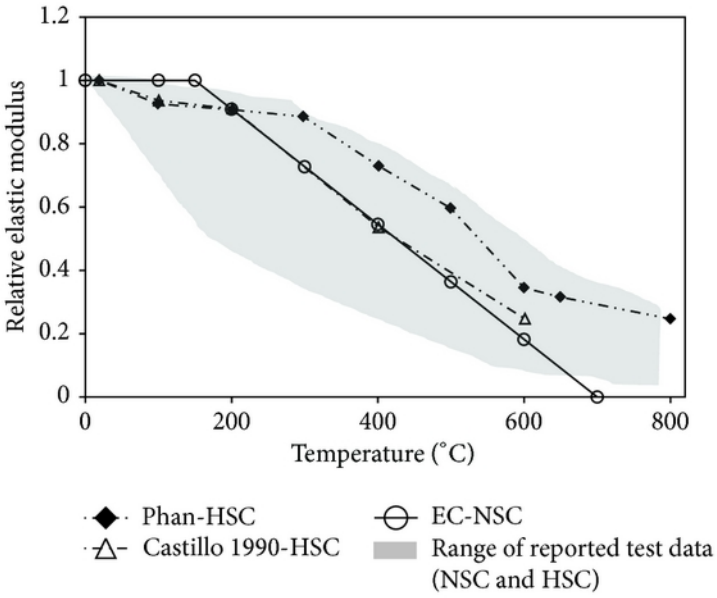

Figure 2.1: Elastic modulus of concrete at elevated temperature. Extracted from (Kodur, 2014)

strength of UHPFRC for both cold and hot-cured concrete was found to increase up to 400^oC and started decreasing afterwards (see Figure 2.2). The relative residual strength was defined at a given temperature (T) as the ratio of the residual strength (f_{ck-T}) to the ambient temperature compressive strength (f_{ck-20}).

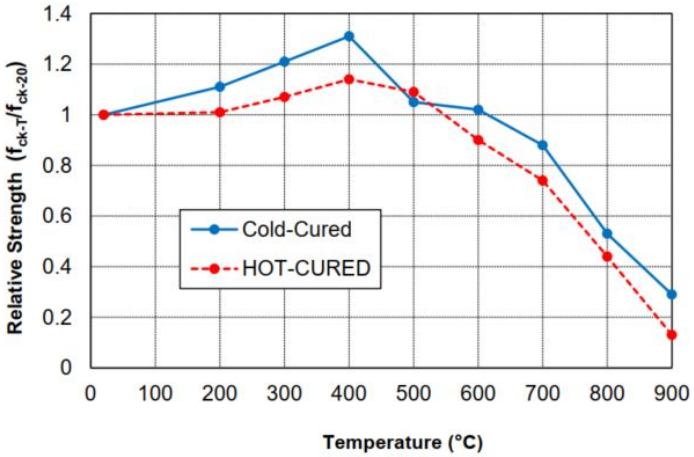

Figure 2.2: Relative residual compressive strength of UHPFRC at elevated temperature. Extracted from (Kahanji, 2016)

2.3.2.4 Tensile strength

In most designs, the tensile strength of concrete is ignored (conservative assumption) but when it is necessary to account for the tensile strength, the EN 1992-1-2 (2008) recommends reduction factors $k_{c,t}$ be multiplied to the tensile strength at ambient temperature to account for the reduction due to elevated temperature effects. Figure 2.3 depicts the evolution of this strength reduction factor as a function of temperature. The tensile strength is maintained up to 100^oC and reduces linearly until all the tensile strength is lost at 600^oC.

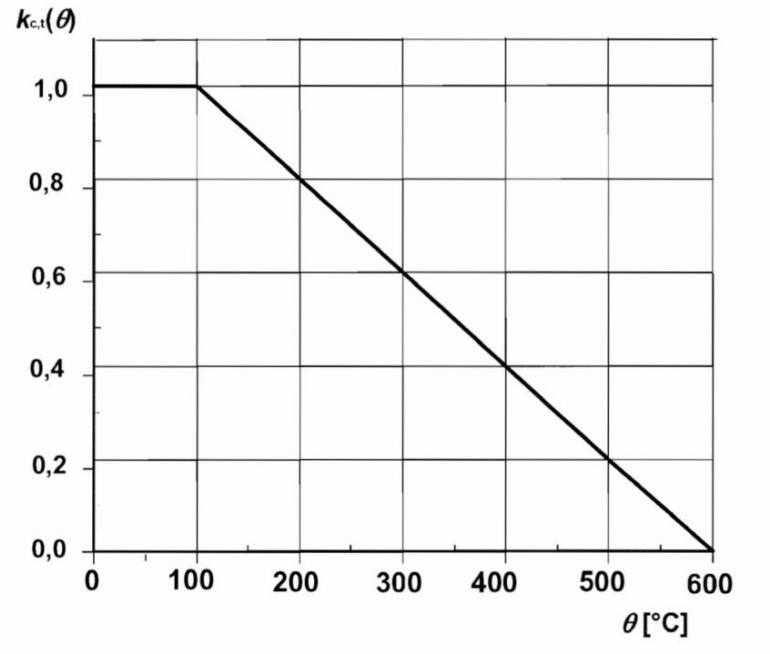

Figure 2.3: Tensile reduction factors of HSC at elevated temperature. Extracted from (EN 1992-1-2, 2008)

2.3.3 Thermal properties

2.3.3.1 Thermal conductivity

The thermal conductivity of concrete is a function of temperature and depends on aggregate and material density. Despite the expected difference in thermal conductivity between NSC and HPC, the thermal conductivity of plain and fibre reinforced concrete do not differ significantly (Kodur and Dwaikat, 2008). EN 1992-1-2 (2008) documents values of thermal conductivity of concrete as function of temperature in terms of

equations and graphs. The equations presented below are given for the upper (Equation 2.3.5) and lower limits of the thermal conductivity (Equation 2.3.6).

The upper limit of thermal conductivity, k, of concrete

For $0^oC \leq \theta \leq 1200^oC$

$$k(\theta) = 2 - 0.2451\left(\frac{\theta}{100}\right) + 0.0107\left(\frac{\theta}{100}\right)^2 \text{ [W/m.K]} \tag{2.3.5}$$

The lower limit of thermal conductivity, k, of concrete

For $0^oC \leq \theta \leq 1200^oC$

$$k(\theta) = 1.36 - 0.136\left(\frac{\theta}{100}\right) + 0.0057\left(\frac{\theta}{100}\right)^2 \text{ [W/m.K]} \tag{2.3.6}$$

where k is the thermal conductivity and θ is the temperature. This relationship between thermal conductivity and temperature is expressed in graphical form as shown in Figure 2.4 below.

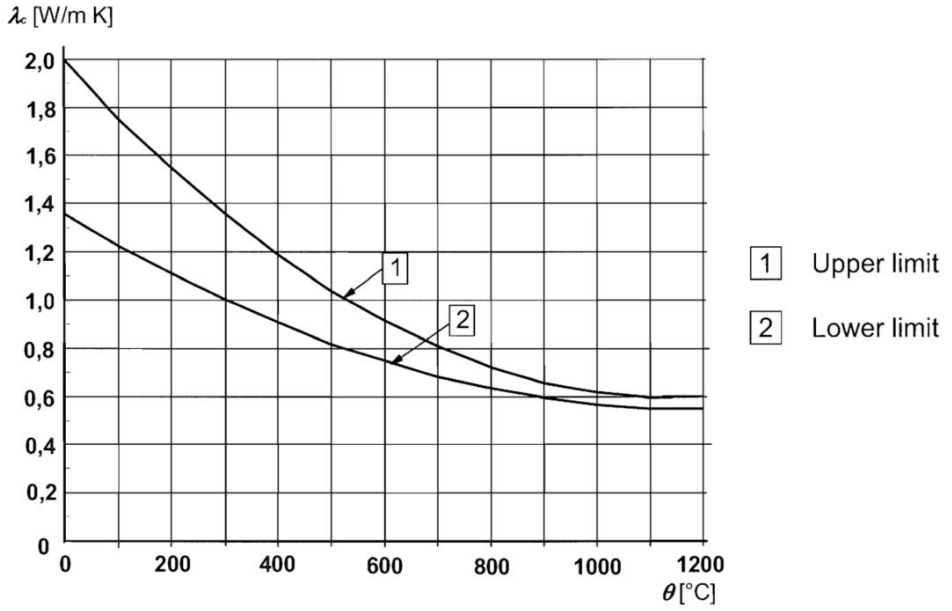

Figure 2.4: Thermal conductivity of concrete at elevated temperature. Extracted from (EN 1992-1-2, 2008)

2.3.3.2 Specific heat capacity

The specific heat capacity, c_p is also based on the expressions suggested in EN1992-1-2 (see Equations 2.3.7 - 2.3.10). This relationship has also been shown in Figure 2.5 for concrete with siliceous and calcareous aggregates at different levels of moisture contents (0, 1.5 and 5%). More details regarding the relationship between moisture content and constant specific heat capacities are given in the code (EN 1992-1-2, 2008).

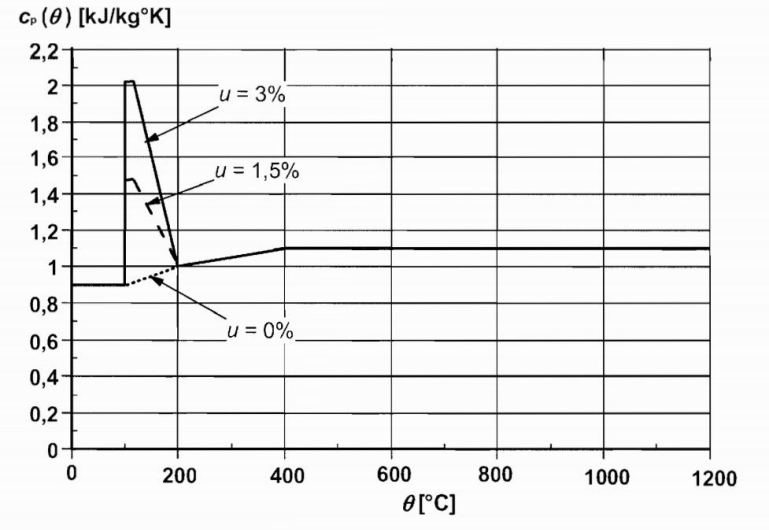

Figure 2.5: Specific heat capacity of concrete at elevated temperature. Extracted from (EN 1992-1-2, 2008)

For $20^o \leq \theta \leq 100^o$

$$c_p(\theta) = 900 \text{ [J/Kg.K]} \tag{2.3.7}$$

For $100^o \leq \theta \leq 200^o$

$$c_p(\theta) = 900 + (\theta - 100) \text{ [J/Kg.K]} \tag{2.3.8}$$

For $200^o \leq \theta \leq 400^o$

$$c_p(\theta) = 1000 + \left(\frac{\theta - 200}{2}\right) \text{ [J/Kg.K]} \tag{2.3.9}$$

For $400^o \leq \theta \leq 1200^o$

$$c_p(\theta) = 1100 \text{ [J/Kg.K]} \tag{2.3.10}$$

2.4 Fire resistance of concrete structures

Fire is one of the most severe conditions which may be encountered by a reinforced concrete (RC) structure during its lifetime. Therefore, the need to quantify the fire resistance of RC members is an important issue that need to be taken into consideration in the design of RC buildings. Kahanji (2016) defines fire resistance of a member as its ability to withstand the effects of a fire while performing its designed function for a considerable period. In the quantification of fire resistance of structural elements, two design approaches are commonly employed, and these are: *prescriptive approach*, and *performance-based approach*.

2.4.1 Prescriptive design

The prescriptive approach is employed in a number of current design standards, such as EN 1992-1-2 (2008), BS 476-22 (1987) and ACI/TMS Committee 216 (1997) for estimation of fire resistance of RC members. This approach is a tabulated method which specifies some deemed-to-satisfy requirements of the minimum member dimensions and minimum concrete for the reinforcing steel bars. The requirements stipulated in tables are derived from empirical approaches and heavily relies on limited fire resistance test results of RC members where the RC member is pre-loaded and then exposed to a prescribed fire curve as defined by ASTM E119-20 (2020), ISO 834-1 (1999), or BS 476-22 (1987).

Despite not being based on accurate understanding of the thermo-mechanical behaviour of RC members exposed to fire, the prescriptive approach generally results on conservative designs. In addition, this approach provides little understanding into the effects of many important factors, such as, load level, geometrical configuration, boundary conditions, temperature-dependent properties, acceptable limit states for RC members exposed to fire, and cracking and stiffening behaviour of concrete (Kodur et al., 2008; Purkiss and Li, 2013).

2.4.2 Performance-based design

Due to the limitations of the prescriptive approach, recent years has seen a gradual drift towards performance-based design in structural fire design of RC members. In addition to its ability to allow designers to use multiple routes to achieve the required level of safety, this drive has been due to the cost-effectiveness, flexibility and rationality of the performance-based approach (Hurley and Rosenbaum, 2019). The growing need for performance-based fire safety design has led to the development of tools, with the desired capabilities, for the accurate fire resistance analysis of RC members. The development of such a tool in the context of UHPFRC beams is the objective being achieved in this study.

2.5 Numerical approach to performance-based design

2.5.1 Introduction

Concrete members have an outstanding fire resistance. However, at elevated temperatures its mechanical and thermal properties degrade with temperature. Therefore, concrete structures should be designed to withstand fire for a considerable period while performing its function. The goal of structural fire design is to estimate the fire resistance of a member which is defined as the ability of a member to resist fire performing its intended function for a given period of time. As discussed in the previous section, performance-based design in getting more attention in structural fire engineering. Its details are given in this section.

The general procedure for performance-based structural fire design involves three steps: fire modelling; heat transfer modelling; and structural analysis (Parkinson et al., 2008)

2.5.2 Fire scenario analysis

One possibility of accounting for thermal action on structures subjected to fire is by use of time-temperature curves. These curves describe how gas temperature around a

structure evolves with time (Franssen and Real, 2016). EN 1992-1-2 (2008) considers three different time-temperature curves.

The *standard ISO 834 fire curve* is the oldest fire curve which is still used even today to rate structural elements in fire tests. The ISO834 curve is given by equation below:

$$\theta_g = 20 + 345\log_{10}(8t+1) \tag{2.5.1}$$

Where θ_g is the gas temperature in ^oC and t is the time in minutes or hours. Kahanji et al. (2016) used this time temperature curve to model the fire in the furnace.

The *hydrocarbon time-temperature curve* is another fire curve used for representing hydrocarbon type fires mostly experienced in industries. The equation for the hydrocarbon fire is given below:

$$\theta_g = 20 + 1080(1 - 0.325\exp^{-0.167t} - 0.675\exp^{-2.5t}) \tag{2.5.2}$$

The third one is the *parametric time-temperature curve* which is a special type of fire curve that gives the evolution of gas temperature in a compartment as a function of the most important physical parameters that affects how a fire develops in a compartment.

According to Buchanan and Abu (2017), the Eurocode parametric equation for temperature is given for both the *heating phase*, and the *cooling phase*.

2.5.2.1 Heating phase

The temperature $\theta_g(^oC)$ of the heating phase equation is given by:

$$\theta_g = 20 + 1325(1 - 0.324\exp^{-0.2t^*} - 0.204\exp^{-1.7t^*} - 0.472\exp^{-19t^*}) \tag{2.5.3}$$

Where t^* is the fictitious time given by

$$t^* = \Gamma t \tag{2.5.4}$$

And t is the time in hours and

$$\Gamma = \frac{(O/0.04)^2}{(b/1160^2)} \tag{2.5.5}$$

Where O is the ventilation factor and b is a factor that accounts for the thermal properties of the enclosure. The heating phase duration t_d is given by,

$$t_d = \frac{0.0002 e_t}{O} \tag{2.5.6}$$

Where e_t is the fuel load density.

2.5.2.2 Cooling phase

The cooling phase temperature (^oC) is given by:

$$\theta_g = \begin{cases} \theta_{max} - 625(t^* - t^*_{max}x) & \text{for } t^*_{max} \leq 0.5 \\ \theta_{max} - 250(3 - t^*_{max})(t^* - t^*_{max}x) & \text{for } 0.5 < t_{max} < 2.0 \\ \theta_{max} - 250(t^* - t^*_{max}x) & \text{for } t_{max} > 2.0 \end{cases}$$

$$\theta_g = \begin{cases} \theta_{max} - 625(t^* - t^*_{max}x) & \text{for } t^*_{max} \leq 0.5 \\ \theta_{max} - 250(3 - t^*_{max})(t^* - t^*_{max}x & \text{for } 0.5 < t_{max} < 2.0 \\ \theta_{max} - 250(t^* - t^*_{max}x) & \text{for } t_{max} > 2.0 \end{cases}$$

Where $t^*_{max} = (0.0002 e_t / O)\Gamma$ and

$$x = \begin{cases} 1.0 & \text{for } t_{max} > t_{lim} \\ t_{lim} \cdot \Gamma / t^*_{max} & \text{for } t_{max} = t_{lim} \end{cases} \tag{2.5.7}$$

Another possibility of representing fire or thermal actions are the so called natural fire models and these include: zones models, computational fluid dynamics models and localised fires. These models are more accurate than the time-temperature curves but they come at a modelling and computational cost (Kallada and Hostikka, 2019). In

structural design practice, engineers prefer the use of the comprehensive parametric fire curve which is less computationally expensive when it comes to building fire modelling (Ariyanayagam and Mahendran, 2013).

2.5.3 Heat transfer analysis

There are basically three modes of heat transfer: radiation, convection and conduction. As the gas temperature in the compartment is changing due to the fire, the temperature of a given structural element in that compartment changes as result of the transfer of heat from the fire to the element by radiation and convection. The heat then travels through the section by conduction.

2.5.3.1 Radiation

Heat transfers by radiation is through electromagnetic waves without the need of a medium (Babrauskas, 2016). The heat energy release by radiation can pass through a perfect vaccum and through air. The amount of heat flux emitted from a real surface by radiation is given by,

$$\dot{q} = \varepsilon_s \cdot \sigma \cdot T_s^4 \tag{2.5.8}$$

Where ε_s is a dimensionless quantity which is called the emissivity of the surface, T_s is the fire temperature in Kelvins and σ is *Stefan-Boltzmann constant* and $\sigma = 5.670 \cdot 10^{-8} W/(m^2 K)$.

On the other hand, given two surfaces which are assumed to be parallel planes, Clause 3.1(6) of EN 1992-1-2 (2008) gives an expression for calculating net radiative heat flux per unit surface area $\dot{h_{net,r}}$:

$$\dot{h_{net,r}} = \Phi \cdot \varepsilon_m \cdot \varepsilon_f \cdot \sigma[(\Theta_r + 273)^4 - (\Theta_m + 273)^4] \tag{2.5.9}$$

Where ϕ is the configuration factor, ε_m is the emissivity of the member which is specified to be 0.8 in EN 1991-1-2, ε_f is the emissivity of the fire which is specified to be 1.0 in EN 1991-1-2, σ is Stefan-Boltzmann constant ($\sigma = 5.670 \cdot 10^{-8} W/(m^2 K)$, Θ_r is the effective radiation temperature of the compartment [^oC], and Θ_m is the effective

radiation temperature of the member [^oC].

2.5.3.2 Convection

Heat moves by convection from a fluid to a surface of a solid when the two are at distinct temperatures. The most important property in Structural Fire Engineering when estimating heat transfer by convection is the convection heat transfer coefficient, usually denoted by h_c.
There are many methods for estimating h_c but Clause 3.1(6) of EN 1992-1-2 (2008) gives the formula for net radiative heat flux by convection:

$$\dot{h_{net,c}} = h_c \cdot [\Theta_g - \Theta_m] \tag{2.5.10}$$

Where h_c is the coefficient of heat transfer by convection $[W/m^2K]$, Θ_g is the gas temperature in the vicinity of the fire exposed member, $[^oC]$, Θ_m is the surface temperature of the member$[^oC]$. For exposed surfaces, the convection heat transfer coefficients of $25W/m^2K$ and $50W/m^2K$ are prescribed in EN 1992-1-2 (2008) for the ISO834 and hydrocarbon fire curves, respectively where as for unexposed surfaces the convective heat transfer coefficient is prescribed as $9W/m^2K$ for both the the ISO834 and hydrocarbon heating regimes.

2.5.3.3 Conduction

The concept of heat transfer by conduction occurs at molecular level when molecules with high thermal energy transmit this energy to molecules with low energy (Buchanan and Abu, 2017). For conduction in one dimension, Fourier's law state that the heat flux $\dot{q}''$ is given by,

$$\dot{q_i} = -k \cdot T_{,i} \tag{2.5.11}$$

Where i is the i^{th} spatial coordinate, k is the thermal conductivity of the material, T is the temperature, and T,i is the derivative of the i^{th} spatial coordinate.

2.5.4 Structural analysis and design

Structural analysis involves the determination of displacements and internal forces in members of structures subjected to a range of loads which include among others: dead loads, live loads, wind load, thermal loads, earthquake loads, blast load e.t.c. For structural fire design, mechanical loads (dead and live loads) and thermal loads are usually encountered (EN 1992-1-2, 2008). Based on these internal shear forces, bending moments and displacements can be estimated by either first order linear elastic analysis, second order analysis or by plastic analysis depending on the type of material and structural member being analysed (EN 1992-1-2, 2008).

After determination of applied internal forces, the structure and its structural members are then designed to resist the applied forces (EN 1992-1-2, 2008). This can be done by either following prescriptive provisions or using performance based approach (Bachman et al., 2018). Prescriptive provisions are documented in codes of practice and the most recent codes are based on the limit state design philosophy where the member being designed has to satisfy both ultimate limit states (ULS) and and serviceability limit state (SLS) (EN 1992-1-2, 2008; EN 1992-2, 2005)).

2.5.5 Fire resistance rating

A concrete element is given a fire resistance rating based on a standard furnace (ISO 834 fire curve) test results or using the performance based design procedure described previously (BS 476-22, 1987; Hurley and Rosenbaum, 2019). The members are rated based on achieving some limit state. The three limit states to which structural members are rated for fire include: integrity, insulation and stability.

2.5.5.1 Integrity (E)

This is estimated as the time it takes for the integrity of the element to be maintained while the element is still performing its separating function. This is fundamentally the time it takes until the unexposed surface starts to malfunction or deform as a result of flaming.

2.5.5.2 Insulation (I)

This is estimated as the time it takes before the unexposed surface or a point on the unexposed surface exceeds a specified temperature. For standard fire rating, a temperature of 140^{o}C is the limit specified by EN 1992-1-2 (2008), as most materials no longer provide any insulation when temperatures are above 400^oC.

2.5.5.3 Stability (R)

This refers to the time it takes for the structural element to maintain its load-bearing function during a fire. In most codes of practice, deflection is used to define the load-bearing function for flexure members. In such a case, the fire rating of the member, will be the time it takes for the member to exceed a given deflection limit during a fire scenario. Limiting deflection that define failure are set out in two standards; the BS 1363-1 and the BS 476-20. The threshold deflection prescribed by the BS 1363-1 standard is ($L^2/400d$) while that prescribed by the BS 476-20 is (L/20), where L is the span and d is the effective depth.

2.6 Previous studies on numerical modelling of concrete for fire

There has been a number of research efforts towards the development of numerical simulation tools for fire resistance analysis of concrete structures. Such studies notably focusing on NSC and UHPFRC beams, are discussed in the following paragraphs. In some of the studies the concrete beams were thermally insulated with externally bonded fibre-reinforced polymers (EBR-FRP) strips.

2.6.1 NSC beams

Ellingwood and Lin (1991) conducted an experimental and numerical study to investigate the flexural and shear behaviour of concrete beams during fires. In their study, six two-span continuous beams, four of which were exposed to ASTM E119 fire and

two of which were subjected to a short-duration high intensity (SDHI) natural fire, were fabricated. Numerical models were developed for the beams and these were used to predict the thermal and structural response of the beams under fire. The accuracy of the models implied that the models were useful for limit state fire design of concrete beams.

Huang and Platten (1997) formulated a non-linear finite element procedure for predicting the behaviour of planar reinforced concrete members subjected to a fire. Their procedure was based on the iterative secant stiffness formulation and all the thermo-mechanical features except spalling required to simulated fire behaviour such thermal expansion, creep, cracking and temperature-dependency of material properties were taken into consideration. Their numerical models were validated by comparing to experimental results.

Capua and Mari (2007) developed a numerical model for simulating the thermo-mechanical response of concrete beams under fire, with focus on modelling the bond between concrete and reinforcing steel. The accuracy of the model was validated against experimental results on four full scale beams tested under fire conditions. They pointed out that the bond between concrete and steel has an important influence on the fire resistance of reinforced concrete structures especially at temperatures above 500^oC.

Kodur et al. (2008) established a numerical model for tracing the behaviour of reinforced concrete beams at elevated temperatures with inclusion of a simplified procedure for incorporating the effect of spalling into the model. The model was validated against full-scale fire resistance tests and the researchers highlighted the significance of the type of failure criterion on fire resistance predictions of RC beams.

Gao et al. (2013) are yet other researchers that considered the finite element (FE) modelling of RC beams exposed to fire. Like Kodur et al. (2008), they also paid particular attention to modelling the interfacial bond-slip behaviour. Their numerical model was compared with a number of experimental test results and the good agreement with FE predictions provided a good understanding of the local behaviour of RC beams under fire.

2.6.2 Thermally insulated NSC beams

Two experimental studies by Dai et al. (2015) and Firmo et al. (2015) developed finite element models to capture the behaviour of thermally insulated RC beams. The RC beams were insulated with EBR-FRP strips. Dai et al. (2015) considered the constitutive modelling of concrete, steel and FRP and the bond-slip behaviour of FRP-to-concrete and steel-to-concrete interfaces. The accuracy in the predictions of their model implied its usefulness for predicting safe fire resistance ratings unlike in other studies where perfect bond-slip is assumed.

On the other hand, Firmo et al. (2015) developed two-dimensional FE models to simulate fire resistant tests on insulated EBR-CFRP RC beams by paying particular attention to the variation with temperature of the thermal and mechanical properties of each constituent material and the CFRP-concrete interaction was modelled using bi-linear bond-slip laws calibrated for different temperatures. The good agreement of their model with experimental predictions allowed the possibility of exploiting the thickness of the CFRP bond and investigate the debonding of CFRP from concrete at elevated temperatures. Their study provided useful information for understanding the fire resistance effectiveness of CFRP system for fire protection.

2.6.3 UHPFRC and UHPC

There has been many experimental research efforts on the investigation of fire resistance of UHPC and UHPFRC beams in the past decade. However, numerical studies for simulating the fire behaviour of UHPC or UHPFRC beams are very limited. So far only two studies were identified by the researcher and details of these studies are discussed in the following paragraphs.

Liang (2018) considered meso-scale modelling for heat transfer analysis of steel fibre reinforced concrete (SFRC) and UHPC. In his study, he modelled Delaunay triangulation to generate unstructured mesh for SFRC materials. After validating the model against experimental results, Liang (2018) used the model to study how model thickness affected the thermal conductivity of models with different fibre lengths. The FE simulations were conducted in a finite element analysis (FEA) software ANSYS.

The results from simulations showed that the presence if steel fibres had an impact on the temperature distribution and heat flux vector of SFRC blocks. However, the meso-scale modelling is complicated and requires a lot of computation effort.

Mai et al. (2020) conducted a numerical simulation of UHPFRC frame structure exposed to fire, using the finite element method. According to their results, the three dimensional FE model was able to capture the thermal and mechanical response of UHPFRC frame structure subjected to a natural fire. After validating the FE model with experimental results, the FE model was used to investigate the influence of polypropylene (PP) fibres on the fire resistance of UHPFRC and HSC. The models revealed that PP fibres improves the fire resistance of UHPFRC and HSC.

2.7 ABAQUS sequentially coupled thermal-stress analysis

ABAQUS defines a sequentially coupled thermal-stress analysis (SCTSA) as a general procedure that is conducted in a sequence by first carrying out an uncoupled heat transfer analysis and then a stress/deformation analysis is conducted afterwards (ABAQUS, 2018). This type of procedure is often used when the temperature distribution can be computed without knowledge of the stress/deformation solution. Several researchers have used SCTSA in the recent past to simulate the behaviour of concrete structures subjected to time temperature curves. The first notable one is the study by Chung et al. (2006) where the authors used SCTSA to conduct finite element stress analysis of high strength reinforced concrete columns at elevated temperatures. Another study is the one by Lakhani et al. (2013) in which the authors numerically simulated ASTM E119 and short severe fires on reinforced concrete columns and beams using SCTSA-based FE analysis. In a similar manner, Mago et al. (2014) used SCTSA to numerically simulate the fire resistance of a concrete composite slab. Last but not least, Mai et al. (2020) used ABAQUS SCTSA to conduct a numerical simulation of a UHPFRC frame structure under fire action.

It should be noted that UHPFRC is a relatively new material. Therefore, many of such SCTSA-based FE models that would help in the understanding and estimation of

fire resistance of UHPFRC members are limited. Building on this understanding, this study applies the principles of SCTSA to develop working three FE models that may be used to numerically simulate the fire resistance of UHFRC beams under different conditions.

2.8 Chapter overview

UHPFRF has shown to display favourable mechanical properties at ambient temperature. However, due to inherent fire induced spalling mechanism, there are still a lot of concerns from researchers on the fire resistance of UHPFRC beams. Even when most of the work conducted on the fire performance of UHPFRC has been limited to small elements such as prism, cubes and cylinders, two studies by Kahanji (2016); Banerji et al. (2020) investigated the fire performance of full-scale UHPFRC beams.

In the review, it was pointed out that to make performance-based design possible and inexpensive, the need for numerical tools cannot be ignored. As a results of being a new technology, most numerical tools for performance based fire design have been developed in the context on NSC. Very few studies have applied a numerical approach to investigate the fire performance of UHPFRC beams. With the objective of investigating the fire resistance of UHPFRC beams within the context of performance-based design, developing a numerical model for that purpose is indispensable. Such a model would be able to capture fire scenario analysis, heat transfer analysis and mechanical response analysis. The numerical model and investigations considered in this dissertation provides very useful information about the fire safety of UHPFRC beams in the context of performance-based design.

Chapter 3

METHODOLOGY

3.1 Introduction

The response of UHPFRC beams in fire has been conducted by a previous experimental study (Kahanji, 2016). In the experimental study, nine beams with varying steel fibre dosages and load ratios were tested at elevated temperature in a furnace following an ISO 834 fire model. However, it is not possible to get full insight of the fire behaviour of UHPFRC beams using an experimental approach. This is mainly due to impractical issues such as: it may not be possible from an economic perspective to cast adequate number of beams to study all different kind of behaviours, it may not be practical to place thermocouples or Linear Variable Differential Transducers(LVDTS) in some regions of the beams, and thus it may not be possible to conduct a parametric study. By building on the principle of the finite element method (FEM), this study investigated the fire response of UHPFRC beams subjected to fire scenarios.

This chapter presents the methodology that was adopted for the numerical investigation of UHPFRC beams under ISO 834 fire curve using a FE analysis software package ABAQUS (ABAQUS, 2018). First and foremost, the chapter gives a brief discussion of Kahanji's (2016) experimental setup in Section 3.2. Secondly, ABAQUS sequentially-coupled thermal-stress analysis procedure adopted in this study is presented in Section 2.7. Thirdly, a generalised uncoupled heat transfer three-dimensional (3D) FE model is developed in Section 3.3. Afterwards, a generalised post-heat transfer mechanical 3D FE model is developed in Section 3.4 and then an investigation method-

ology employed in achieving the dissertation's objectives is given in Section 3.5. Last but not least, an overview of the chapter is given in Section 3.6.

3.2 Kahanji's (2016) experimental setup

As earlier indicated, the beams considered for this study's numerical analysis are taken from an experimental study conducted by (Kahanji, 2016). Kahanji's (2016) experimental program was divided into four series: A, B, C and D grouped according to the load ratio applied on the beams. More details regarding these test series can be obtained from Kahanji (2016). Seven different beams are considered for validation of the present finite element model and these include: RLF2-20, RLF4-20, RLF2-40, RLF4-40, RLF2P-40, RLF2-60, and RLF4-60 beams. The beams were subjected to load ratios of 0.2, 0.4 and 0.6. Only the RLF2P-4 beam contained polypropylene fibres and the rest contained steel fibres.

A typical beam specimen had a span of 2.0m and a cross-section of 100$mm \times$ 200mm reinforced at the bottom with two 16mm diameter high yield strength steel rebars. The steel fibre dosage also varied across the beams with volume percentages of 1, 2%, and 4%. In order to measure temperature, thermocouples were placed at various locations of the beams (see Figure 3.1.

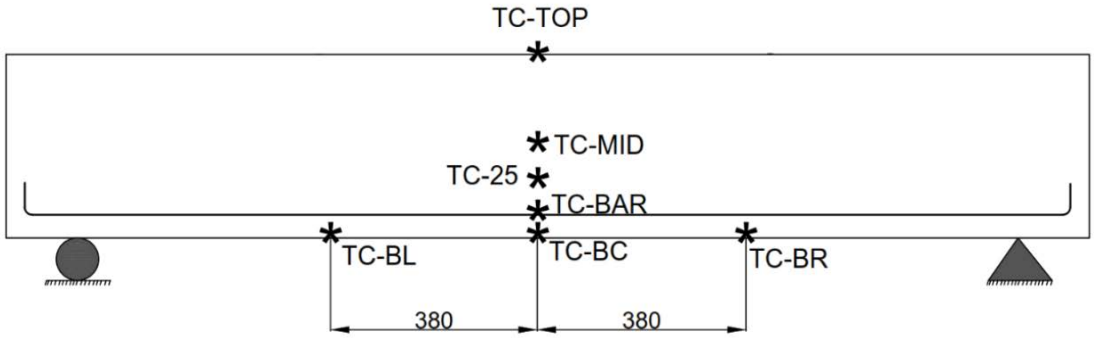

Figure 3.1: Locations of thermocouples. Extracted from (Kahanji, 2016)

The beams were tested in the furnace under the ISO 834-time temperature curve and a depiction of the RLF2-20 beam inside and outside the furnace after the test is shown in Figures 3.2 and 3.3 respectively.

Figure 3.2: RLF2-20 beam inside the furnace after the fire test. Extracted from (Kahanji, 2016)

.

Figure 3.3: RLF2-20 beam outside the furnace after the fire test. Extracted from Kahanji (2016)

.

3.3 Development of a 3D FE model: Uncoupled heat transfer analysis

As previously mentioned in section 2.7, the analysis technique employed in this study is the SCTSA general procedure which consists of an uncoupled heat transfer phase and a subsequent mechanical analysis phase. The uncoupled heat transfer phase is presented in this section. The steps taken to develop a working 3D model for heat transfer simulation are presented.

3.3.1 Analysis procedure

The heat transfer general analysis procedure available in ABAQUS was chosen for the uncoupled heat transfer analysis of UHPFRC beams considered in this study. In order to execute this procedure in ABAQUS, the following decisions were made: the transient response was requested since the temperature development varies with time; the time period was set to 3600 (this being equal to 1 hour of heating with ISO 834 time-temperature curve); a fixed increment size of 5 (maximum allowed time step of 5 seconds as per provisions in (EN 1992-1-2, 2008)) was chosen with the number of maximum number of increments set to 720 ; and lastly, a direct method to solving the system of equations was chosen and full Newton was set as a solution technique.

3.3.2 Interaction properties

When performing a heat transfer analysis of reinforced UHPFRC beams in ABAQUS, convection, radiation and thermal conductance between steel and concrete must be defined. This is made possible by use of the interaction module. Surface film condition interaction type was used to define convection interaction properties on both the assumed exposed and unexposed sides (see Figure 3.4). The exposed and unexposed sides were defined with convective heat transfer coefficients, h_c equal to $25W/(m^2K)$ and $9W/(m^2K)$ respectively (EN 1992-1-2, 2008).

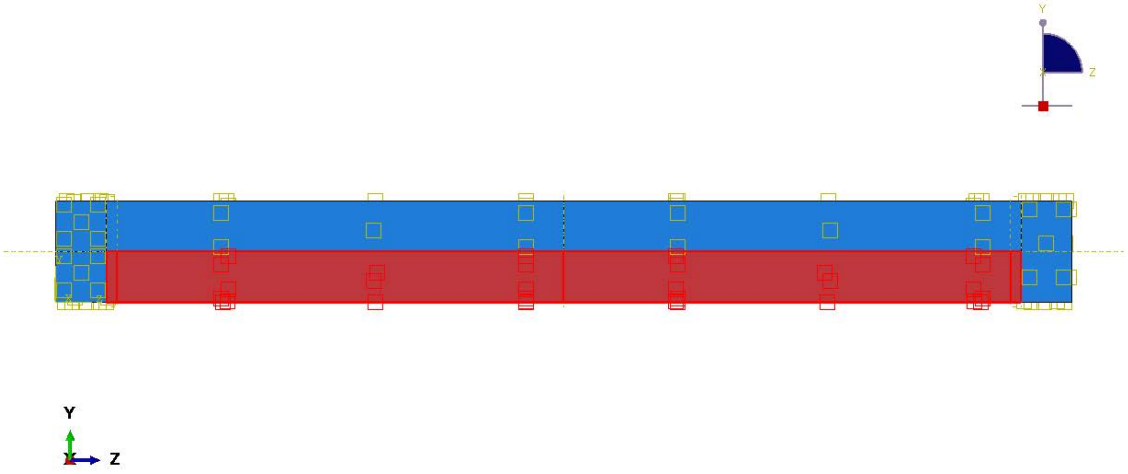

Figure 3.4: [colour] Exposed (red) and unexposed (blue) surfaces

.

ABAQUS's surface radiation interaction type was used to define radiation on the

assumed exposed side of the beam (see Figure 3.4). The radiation type was set to ambient and uniform emissivity distribution with an emissivity of 0.8 was adopted as per Eurocode (EN 1992-1-2, 2008).

In order to simulate heat transfer between concrete and embedded steel reinforcement bar through conduction in ABAQUS, a contact interaction between the two materials was defined. This interaction property was facilitated by defining a thermal conductance interaction property with a thermal conductance of $1000W/K$ for a clearance of $0m$ and a thermal conductance of $0W/K$ for a clearance of $0.002m$.

Having defined the convection, radiation and thermal conductance as described above, the robin boundary conditions required in the formulation of the heat equation were defined.

3.3.3 Loading and boundary conditions

In an uncoupled heat transfer analysis, ABAQUS only requires definition of initial temperature of both the steel and the UHPFRC matrix. This is achieved by creating a predefined temperature field in ABAQUS's load module. The predefined temperature of the whole model was set to ambient temperature (20^oC).

3.3.4 Material properties

3.3.4.1 UHPFRC modelling

In order to model the UHPFRC beams for heat transfer analysis, thermal properties of UHPFRC must be defined. ABAQUS allows definition of material properties through a "create material" tool in the property module. Each material property is defined as a behaviour. For thermal analysis of the beams considered in this study; thermal conductivity, density and specific heat capacity were the required thermal behaviours.

There is a lot of information in literature concerning the temperature dependent thermal conductivity and specific heat capacity of conventional concrete. However, little information is available on UHPFRC. In order to limit the scope on what can be investigated, some of the values recommended by EN 1992-1-2 (2008) for conventional

concrete were adopted.

Lastly, due to limited information on UHPFRC, the temperature-dependent density of conventional concrete reported in EN 1992-1-2 (2008) was adopted for the beams considered in this study and defined appropriately in ABAQUS.

3.3.4.2 Steel reinforcement bar modelling

In the same manner, in order to model the steel reinforcement bar for heat transfer analysis, thermal properties of steel must be defined. ABAQUS allows definition of material properties using a "create material" tool in the property module. Each material property is defined as a behaviour. For thermal analysis of the steel reinforcement bar considered in this study; thermal conductivity, density and specific heat capacity were the required thermal behaviours. The temperature-dependent thermal conductivity, density and specific heat capacity of steel reinforcement bar reported by EN 1993 (2005) were adopted for the beams considered in this study and were defined appropriately in ABAQUS.

3.3.5 Meshing and element types

One of the most crucial steps in applying the finite element method to solve an engineering problem is the discretization of a system into elements called finite elements and selection of element types that closely simulates the actual physical behaviour of the system. ABAQUS provides a variety of element types to use for analyses of different types. However, an ABAQUS analysis will not run or it would give unreasonable results if the wrong choice of element type(s) is made. In this section, the choice of element types for the UHPFRC matrix and the steel reinforcement bar considered in the 3D model for the uncoupled heat transfer analysis is discussed.

3.3.5.1 UHPFRC element types

The UHPFRC was modelled with linear 3D solid tetrahedral elements called 8-node linear heat transfer brick elements. These element types are designated in ABAQUS as DC3D8. They are the most appropriate choice of elements for modelling the 3D

UHPFRC matrix for uncoupled heat transfer analysis. The UHPFRC matrix was seed with a mesh of 0.02 size and a total of 11500 DC3D8 elements were created (see Figure 3.5).

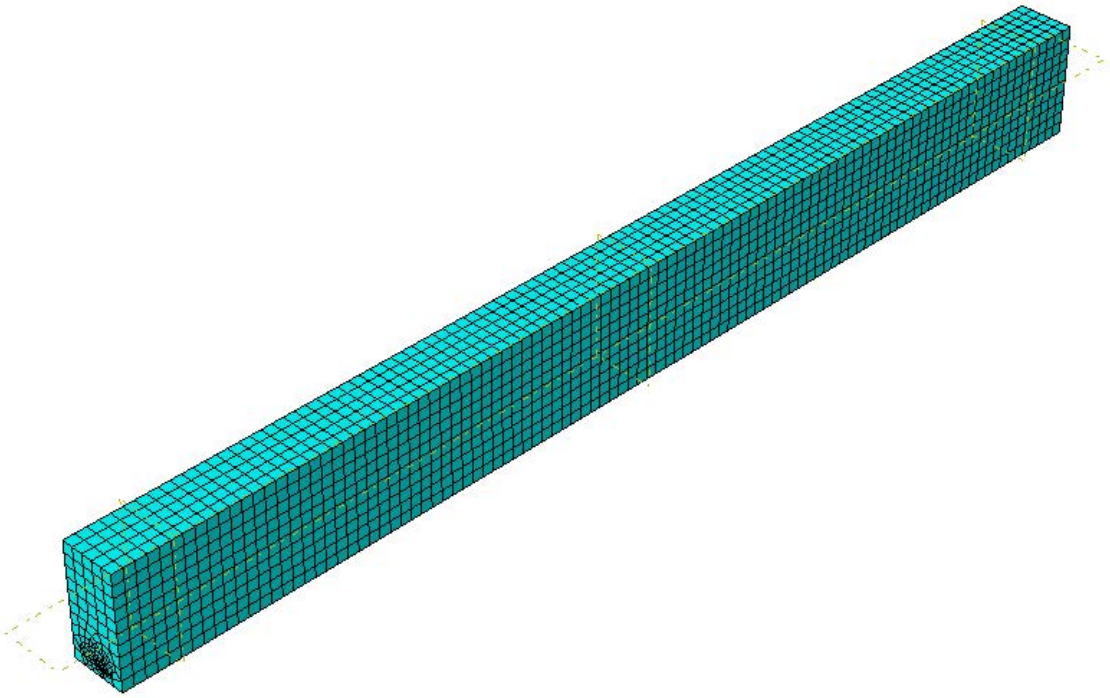

Figure 3.5: UHPFRC matrix meshed with ABAQUS 11500 DC3D8 elements

.

3.3.5.2 Steel element types

The steel reinforcement bars were modelled with linear 3D solid tetrahedral elements called 8-node linear heat transfer brick elements. These element types are designated in ABAQUS as DC3D8. They are the most appropriate choice of elements for modelling the embedded 3D steel reinforcement bar for uncoupled heat transfer analysis. The steel reinforcement bar were seed with a mesh of 0.02 size and a total of 400 DC3D8 elements were created (see Figure 3.6).

Figure 3.6: Steel reinforcement bar meshed with ABAQUS 400 DC3D8 elements

.

3.4 Development of a 3D FE model: Structural analysis

As previously mentioned in section 3.2, the analysis technique employed in this study is the SCTSA general procedure which consists of an uncoupled heat transfer phase and a subsequent mechanical analysis phase. The uncoupled heat transfer phase has been presented in the previous section. Therefore, the subsequent mechanical analysis is considered in this section. The steps taken to develop a working 3D model for the mechanical are discussed. It should be noted, however, that the nodal temperature distribution of the whole model calculated in the uncoupled heat transfer phase are fed into this mechanical analysis and the mechanical properties of the beams are to be defined as temperature dependent.

3.4.1 Analysis type

The general static analysis procedure available in ABAQUS was chosen for the subsequent mechanical analysis of UHPFRC beams considered in this study. This analysis also included gravity explicitly by defining a step for it. In order to execute this procedure in ABAQUS, the following decisions were made: a time period of 1 was defined and analysis defined as a non-linear analysis with automatic stabilization specified with a dissipated energy fraction of 0.0002; automatic incrementation was chosen with the number of maximum number of increments set to 1000; and lastly, a direct method to solving the system of equations was chosen and full Newton was set as a solution technique. Midspan displacement was the requested response of the study.

3.4.2 Interaction properties

When performing a mechanical analysis of reinforced UHPFRC beams after a heat transfer analysis in ABAQUS, perfect bond between the concrete and the steel must be defined. This is made possible by use of the interaction module.

Surface to surface contact interaction type was used to define bond-slip between interaction the concrete and the steel rebars. This was achieved by defining using the Abaqus' "tie-constraint" interaction property which does not allow any relative slip.

3.4.3 Loading and boundary conditions

The experimental beams were simply supported and therefore, pinned supports at the ends of the beams were defined. Apart from that, the experimental beams were subjected to midspan point loads of $25kN$,$50kN$ and $75kN$ for 0.2, 0.4 and 0.6 load ratios respectively. the load ratios are a percentage of the load capacity of the beam tested at ambient temprature using four point loading test. Kahanji (2016) reports a load capacity of the beams to be 125kN. The loads were defined in ABAQUS and were applied at midspan to simulate experimental setup.

3.4.4 Material properties

3.4.4.1 UHPFRC modelling

In order to model the UHPFRC beams for post-heat-transfer structural analysis, mechanical properties of UHPFRC must be defined. ABAQUS allows definition of material properties using a "create material" tool in the property module. Each material property is defined as a behaviour. For post-heat-transfer structural analysis of the beams considered in this study; elastic modulus, Poisson's ratio, density, compressive strength, and tensile strength were the required mechanical behaviours. The compressive and tensile properties are defined using one of ABAQUS's plasticity constitutive model called Concrete Damage plasticity (CPD).

There is a lot of information in literature concerning the temperature dependent mechanical properties of conventional concrete. However, little information is available

on UHPFRC. In order to limit the scope on what can be investigated, values recommended by EN 1992-1-2 for conventional concrete and some from some studies on HSC/UHPFRC were adopted. These properties are presented in Chapter 2.

3.4.4.2 Steel reinforcement bar modelling

The following mechanical properties were used to model the behaviour of steel reinforcement bar; elastic modulus, Poisson's ratio, density,and plasticity. The temperature-dependent elastic modulus, density, and plasticity of steel reinforcement bar reported in chapter 2 were adopted for the beams considered in this study and were defined appropriately in ABAQUS. For simplicity, the plasticity behaviour captured the strain at yield point and strains in the plastic region were not captured, as this would have led to time-consuming non-linear calculations.

3.4.5 Meshing and element types

In this section, the choice of element types for the UHPFRC matrix and the steel reinforcement bar considered in the 3D model for the post-heat transfer mechanical analysis is discussed.

3.4.5.1 UHPFRC mesh type

The UHPFRC was modelled with linear three-dimensional solid tetrahedral elements called 8-node linear brick elements with reduced integration and hourglass control. These element types are designated in ABAQUS as C3D8R. They are the most appropriate choice of elements for modelling the three-dimensional UHPFRC matrix for 3D mechanical stress analysis. The UHPFRC matrix was seed with a mesh of 0.02 size and a total of 11500 C3D8R elements were created.

3.4.5.2 Steel mesh type

The steel rebars was modelled with linear 3D solid tetrahedral elements called 8-node linear brick elements with reduced integration and hourglass control. These element

types are designated in ABAQUS as C3D8R. They are the most appropriate choice of elements for modelling the 3D steel reinforcement bar for 3D mechanical stress analysis. The steel reinforcement bar were seed with a mesh of 0.02 size and a total of 400 C3D8R elements were created .

3.5 Investigation methodology

3.5.1 Beams considered

As earlier indicated, the beams considered in this study are adapted from Kahanji (2016) study. However, not all beams were compared with the developed FE model but the only beams that were compared are those in the experimental series A, B and C (Kahanji, 2016). The numerical results obtained in this study were compared to the test results reported on these eight beams. The results and the comparisons are presented in the next chapter.

3.5.2 Validation of the models

Using the experimental data obtained on the eight beams to be considered, the developed FEM models are validated in terms of thermal and mechanical response. As presented in the results chapter, the developed FEM models predict temperature distributions and subsequent deflections which are in close agreement with the experimental data reported by Kahanji (2016). This implied that the developed FEM models according to the approach described in this chapter are valid and can be used for further fire resistance analyses.

3.5.3 Fire resistance of beams

After validating the FEM models developed in this section, it was necessary to use the validated models to conduct a fire resistance parametric study. In the parametric study, two parameters were investigated, that is, the heating regime and load levels. The heating regime compared temperature distributions from the ISO 834 curve and

the hydrocarbon curve. The load ratios were varied from 0.1 to 0.9 and corresponding deflections were predicted and used for estimating the fire resistance of UHPFRC beams. The results of the parametric study are presented in section 4 of the results chapter.

3.6 Chapter overview

This chapter presented a methodology that was adopted in order to achieve the objectives of this study. The chapter presented Kahanji's (2016) experimental setup so as to set a stage for the designation of the beams to be studied using this study's numerical approach. Then the use of sequentially coupled thermal stress analysis in ABAQUS was introduced as an appropriate method for this study's investigation. The methodology used in the development of the two 3D FEM models for uncoupled heat transfer and mechanical analysis in ABAQUS was described and an investigation methodology to which the results are presented in the next chapter was also discussed. Having developed the two FE models, analysis of the thermal and mechanical response can be discussed and this information is given in the next chapter.

Chapter 4

RESULTS AND DISCUSSION

4.1 Introduction

Sequentially coupled thermal-stress finite element models were developed using the methodology described in the previous chapter. In this chapter, the models are compared and validated against experimental results and used for subsequent fire resistance parametric study. The results of the comparisons and the parametric study are presented in this chapter.

This chapter is arranged as follows: predicted and experimental heat transfer response is presented and discussed in Section 4.2, the predicted and experimental structural response is presented in Section 4.3, a fire resistance parametric study utilising the validated FEM models is presented in Section 4.5 and an overview to this Chapter is given in Section 4.6.

4.2 Heat transfer analysis

4.2.1 Temperature distribution

The full-scale 3D finite element model after 60 minutes of exposure to the ISO 834 fire curve is presented in Figure 4.1 The simulated results showing temperature development of the half length of the beam at 1, 15,30,45 and 60 minutes are shown in Figure 4.2.

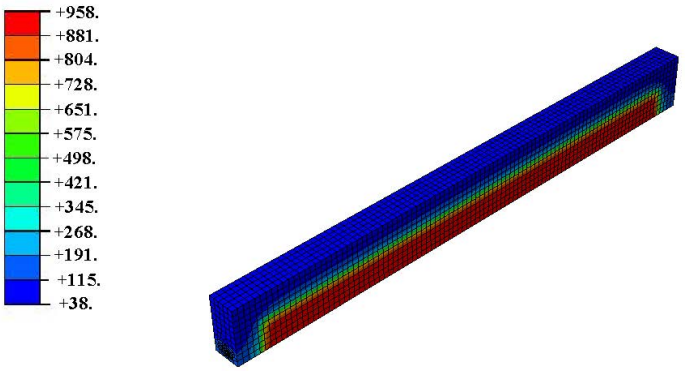

Figure 4.1: full size FE model of the beam after 60 minutes of ISO-834 fire.

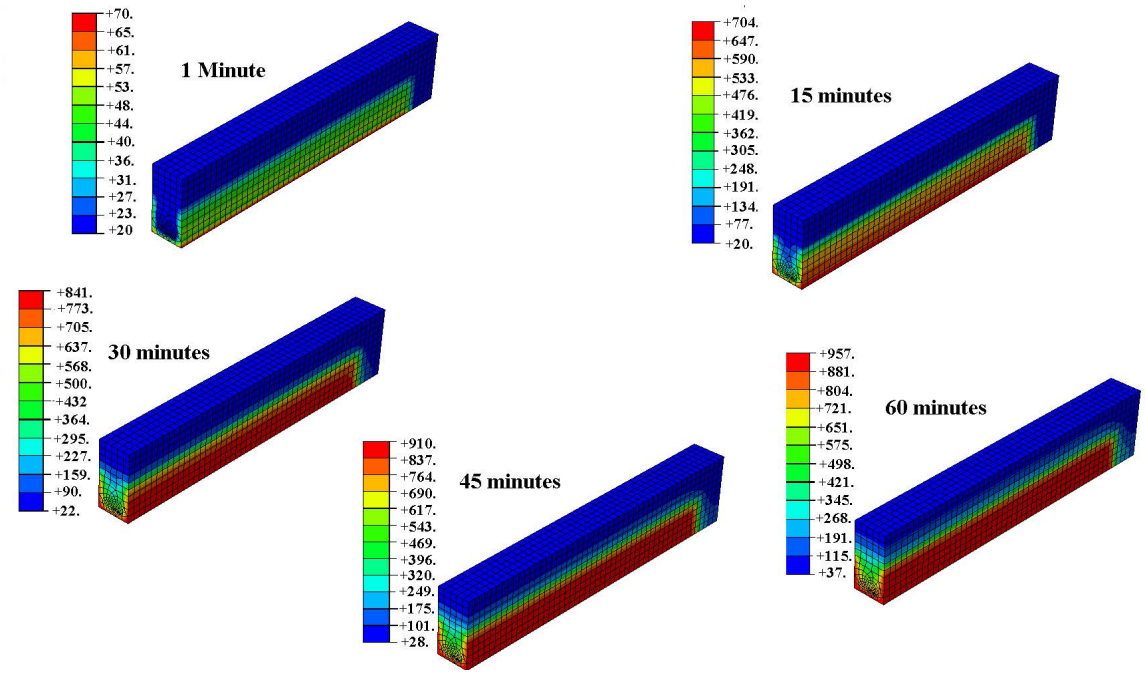

Figure 4.2: Half-size models of the beam simulating temperature development at different times.

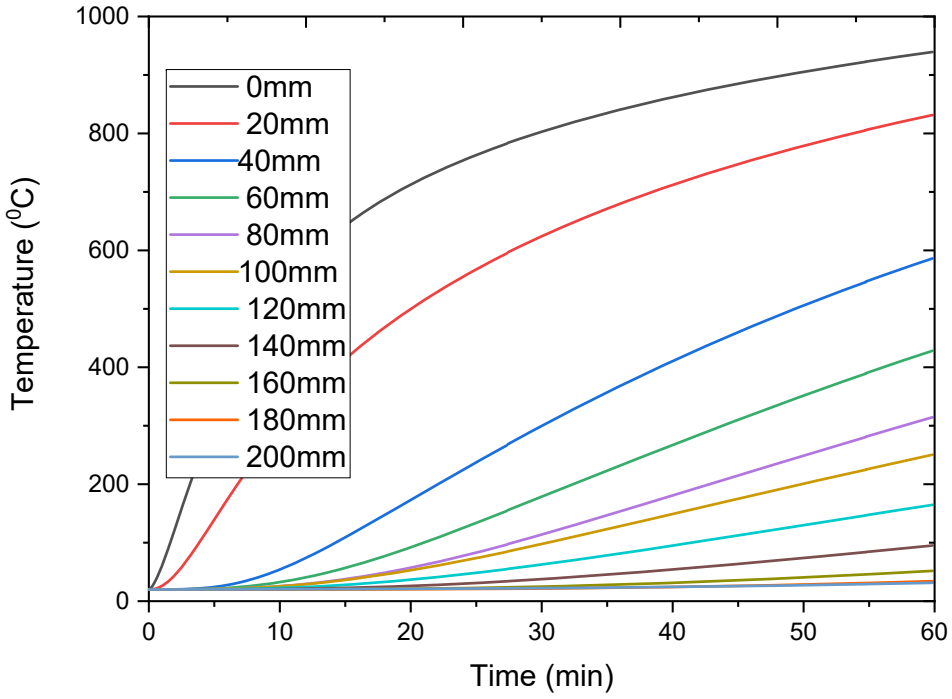

Figure 4.3: Predicted temperature distribution at various depth at midspan cross-section.

The temperature distribution across the cross-section of the beam's midspan from bottom to the top surface over a duration of 60 minutes is depicted in Figure 4.3. The points across the depth of the section were simulated in increments of 20mm from the bottom surface to the top surface. As expected, the temperature distribution shows higher temperature for points closer to the bottom surface.

4.2.1.1 Temperature distribution at the bottom surface

This section presents a comparison between test and predicted temperature evolution at the bottom surface of the beams. The comparison of FEM model with Kahanji (2016)'s test beams that contained 2 vol. % steel fibres is depicted in Figure 4.4. Apart from the RLF2P-40 beam, the temperature predicted by the FEM model agreed with test results in the initial 15 minutes of the test. However, from 15 minutes up to the end of the test, the temperatures measured from test beams was higher than the those predicted by the FEM model. The discrepancy in the last 45 minutes could be explained in terms of spalling. Kahanji (2016) reported a commencement of spalling in the test beams around

the 15^{th} minute causing the thermocouples to be detached from the bottom surface and starting to record furnace temperature.

The temperatures of the RLF2P-40 test beam were significantly lower at all heating stages except a steep increase in temperature was observed in the last 15 minutes of the test. The temperature at the 60th minute almost matched the predicted temperature. This observation can be explained in terms of the moisture content in the RLF2P-40 test beam. The RLF2P-40 beam was reported to contain high levels of moisture (Kahanji, 2016). Therefore, in the first 45 minutes the moisture was still being driven out by heat resulting in a steep increase of temperature afterwards.

Next, the FEM model with the test beams that contained 4 vol. % fibres are comparedd (see Figure 4.5) . In the initial 15 minutes, the FEM model was in good agreement with all the three test beams. However, after the 15^{th} minute, the thermocouple on bottom surface of the RLF4-40 test beam showed significantly higher temperatures than the predicted values up to the end of the test. This discrepancy can be explained by the detachment of the thermocouples from the bottom surface on the RLF4-40 beam due to spalling, as observed and reported by Kahanji (2016).

On the other hand, Kahanji (2016) reported that thermocouples on the RLF4-20 and RLF4-60 beams remained attached on the beams and hence the good agreement in temperature evolution with predicted temperatures even after the 15^{th} minute. However, the temperature evolution on the RLF4-20 and RLF4-60 beams was slightly higher than the predicted near the end of the test. This could have been attributed to the complete loss of moisture in the beams at the end of the test resulting in a decrease in the specific heat capacity of the concrete matrix. The general agreement of the results from the FEM model and the test beams implies the usefulness of the FEM model for use in parametric fire resistance analysis of UHPFRC beams.

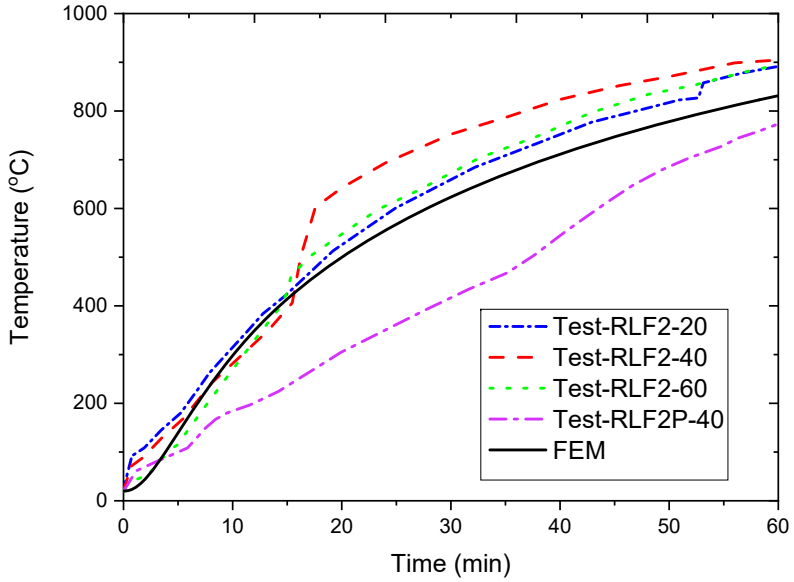

Figure 4.4: Bottom surface temperature evolution of the FE model versus experimental beams with 2 vol. % fibres.

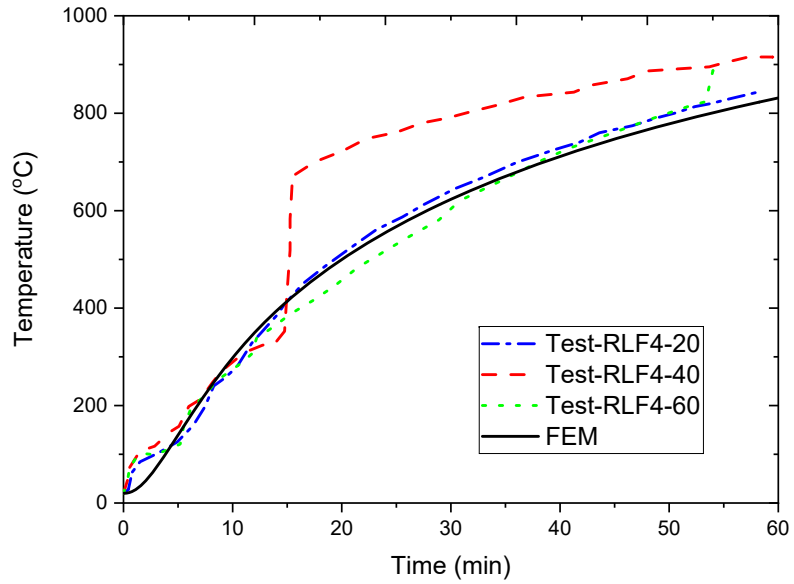

Figure 4.5: Bottom surface temperature evolution of the FE model versus experimental beams with 4 vol. % fibres.

4.2.1.2 Temperature distribution in the steel reinforcement

The measured and predicted rebar temperatures at mid-span in beams with 2 vol. % fibres are plotted in Figure 4.6 as a function of fire exposure time. The measured and predicted show very good agreement in the first 15 minutes of fire exposure. The measured temperatures at the rebar dropped below the predicted after the 15^{th} minute until the end of the test. This may be attributed to the spalling reported around the 15^{th} minute by Kahanji (2016). This can be explained in terms of upward drifting of moisture from the bottom to the concrete around the steel bars. The thermocouple placed at the rebars may have have been disturbed by the explosion inside the concrete due to pore pressures. The lack of agreement between FEM and the RLF2P-40 beam suggests that a model developed with thermal properties accounting for the influence of polypropylene fibres is needed. This would be useful for predicting the fire resistance of such members, which have shown to have a good fire resistance than beams without polypropylene fibres.

The measured and predicted rebar temperatures at mid-span in beams with 4 vol. % are plotted in Figure 4.7 as a function of fire exposure time. Like the beams with 2 vol. % fibres, the measured and predicted show very good agreement in the first 15 minutes of fire exposure but a disagreement can be noticed afterwards. This can be explained in terms of spalling and moisture content. The RLF4-20 beam did not experience significant spalling and hence matched well with the FEM model until 45 minutes of fire exposure. The rise in temperature after the 45^{th} minute can be attributed to exposure of steel due to reduction in the cover as a result of spalling. In general, the FEM model developed predicts the measured results within the required precision and can be used for performance-based fire safety design.

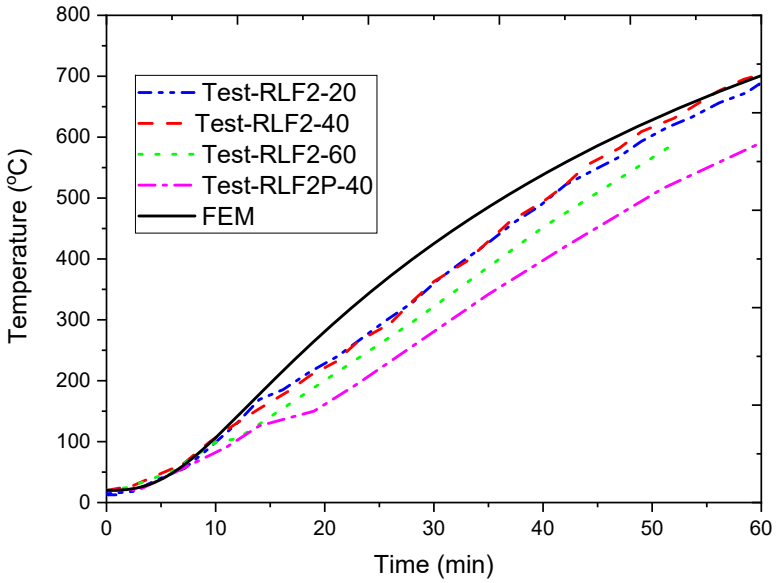

Figure 4.6: Temperature distribution in the steel reinforcement of the FE model versus experimental beams with 2 vol. % fibres.

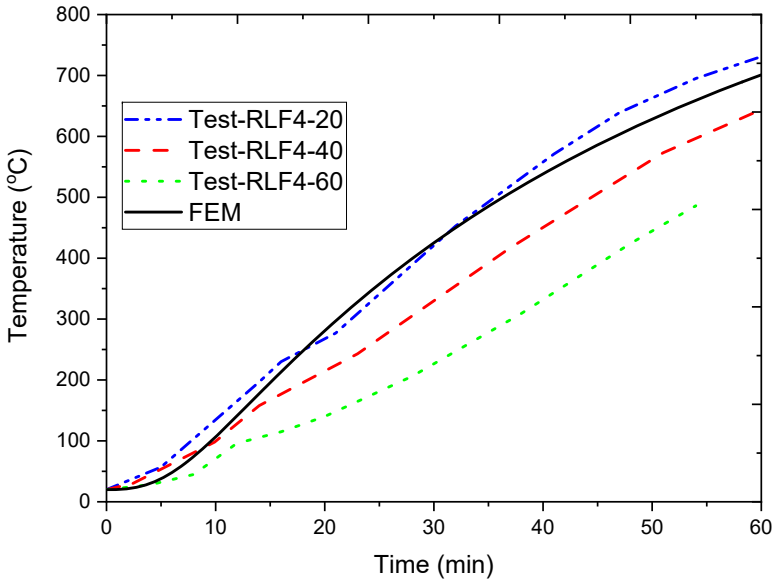

Figure 4.7: Temperature distribution in the steel reinforcement of the FE model versus experimental beams with 4 vol. % fibres.

4.2.1.3 Temperature distribution at the mid-depth

This section presents a comparison between test and predicted temperature distribution at the mid-depth of the beams.

The comparison of FEM model with test beams that contained 2 vol. % steel fibres is depicted in Figure 4.8. The measured temperature distribution of all four beams has been widely dispersed and shows little uniformity due to the varied spalling levels reported by Kahanji (2016). As can be seen in Figure 4.8, temperatures in the first 15 minutes show little dispersion and there is good agreement between test results and predicted results.

The comparison of FEM model with test beams that contained 4 vol. % steel fibres is depicted in Figure 4.9. Unlike, the beams with 2 vol. %, the temperature distribution of the beams with 4 vol. % showed no dispersion. The lack of dispersion was due to non-varying spalling patterns reported by Kahanji (2016) and this implied that an increase in steel fibre dosage guarantees an increase in thermal insulation. The measured and the predicted temperature distribution were in good agreement in the initial 40 minutes but the measured became lower than the predicted after 40 minutes until the end of the test. The fall in temperature could be attributed to the presence of moisture in the test beams, that has the potential to lower the temperature. The increase in moisture content could be explained by the upward drifting of moisture from the bottom surface to the top surface as result of high temperature boundary conditions at the bottom.

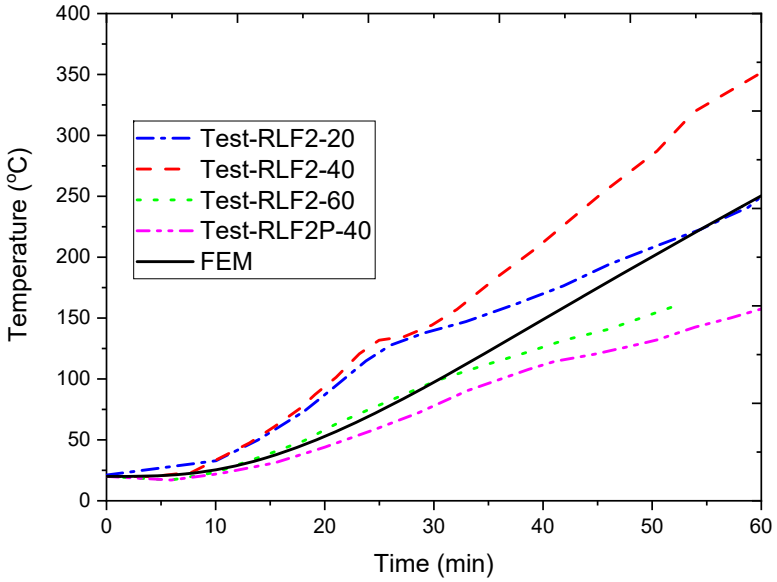

Figure 4.8: Mid-depth temperature evolution of the FE model versus experimental beams with 2 vol. % fibres.

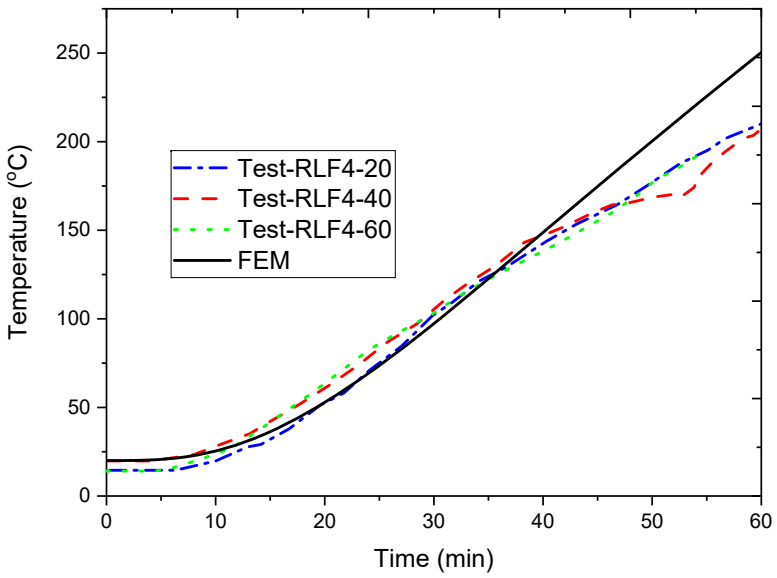

Figure 4.9: Mid-depth temperature evolution of the FE model versus experimental beams with 4 vol. % fibres.

4.2.1.4 Temperature distribution at the top surface

This section presents a comparison between test and predicted temperature distribution at the top surface of the beams. The comparison of FEM model with test beams that contained 2 and 4 vol. % steel fibres is depicted in Figure 4.10 and 4.11, respectively. As can be seen from both figures, the temperature produced by the model matched reasonably well with the temperature reported in the beams. The slightly higher temperatures measured in the beams can be expected, taking into account the fact that some beams had spalled substantially and consequently underwent extreme deflection, which brought the top surface close to the furnace gas temperature. The RLF2-40 was the only exception, as already indicated by the Kahanji (2016), its top surface was basically inside the heated furnace after a failure of 50 minutes, which explains such a substantial increase in temperature reported.

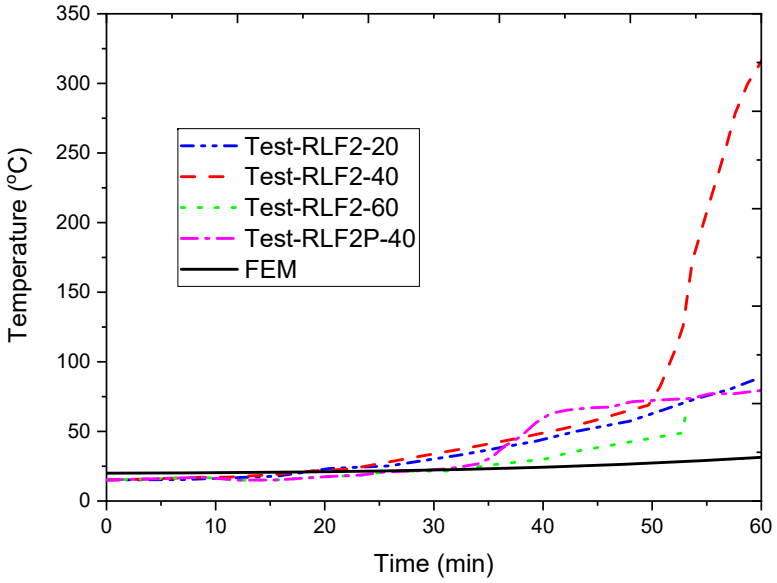

Figure 4.10: Top surface temperature evolution of the FE model versus experimental beams with 2 vol. % fibres.

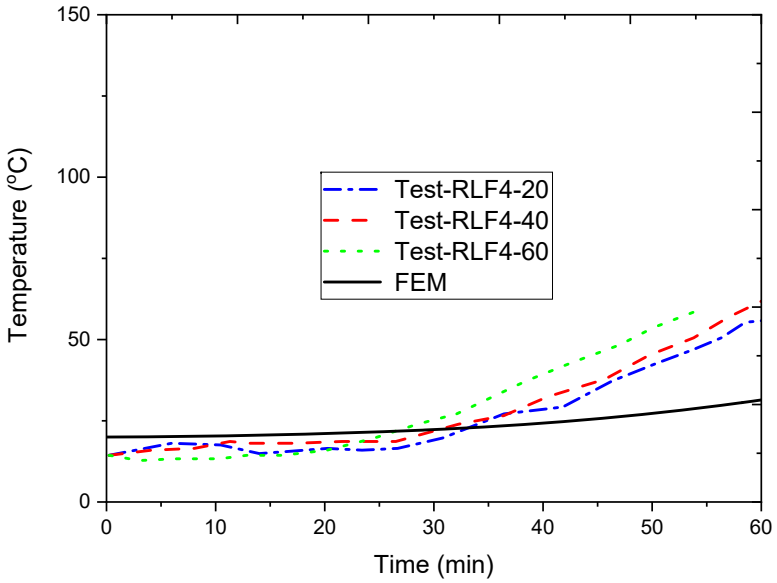

Figure 4.11: Top surface temperature evolution of the FE model versus experimental beams with 4 vol. % fibres.

4.2.2 Temperature distribution over the beam's thickness

In order to assess the fire resistance of a flexural member, it is vitally important to measure temperature across the cross-section of the member over the period of exposure to fire. Figure 4.12 displays predicted temperature distribution across the beam section from the bottom of the exposed surface to the unexposed top surface. The shown temperature distributions shwon were taken at 15, 30, 45 and 60 minutes. The next section compares the temperature distribution predicted and the temperature measured based on the RLF2P-40 beam at the four specified time intervals.

4.2.2.1 FE-Model versus RLF2P-40

Distribution of temperature over the RLF2P-40 beam depth at 15, 30, 45, and 50 minutes were portrayed graphically, and compared to the FEA Temperature of model in Figures 4.13 - 4.16. It can be shown that the temperature difference between the observed and the predicted values at the exposed surface was initially wider and then narrowed with the exposure period. As previously observed, the RLF2P-40 had large amounts

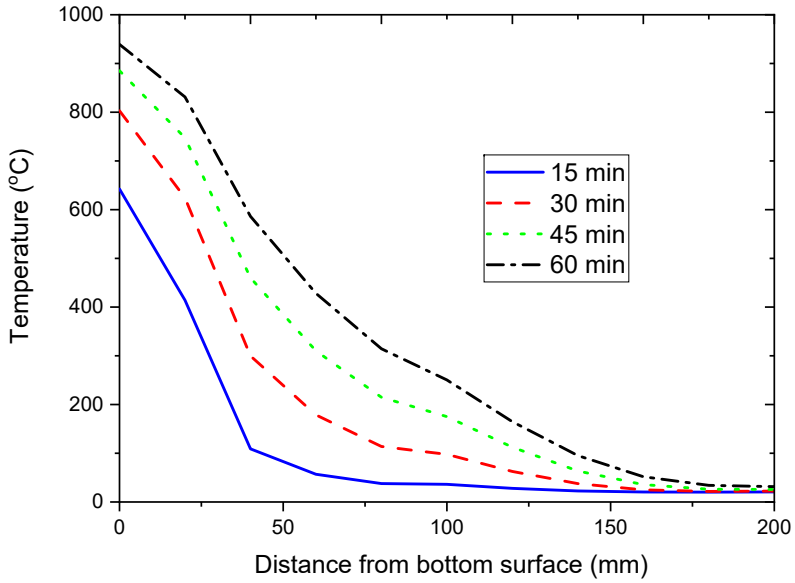

Figure 4.12: Temperature distribution across the beam's depth from exposed surface.

of moisture. Usually, the desorption of moisture occurs on the surface of the material when exposed to heat. This desorption helps to avert temperature rises.

Nonetheless, as heating continued, more and more humidity evaporated and the overwhelming amount of it plummeted to the top surface, so the temperature measured closely matched that of the model at those locations with reduced moisture. For example, at 15 minutes the difference on the bottom surface (0 mm) between the measured and the predicted temperature was about 120^o C but at 60 minutes it was reduced to about 30^o C. The moisture phase that drifted to the upper regions of the beam caused the temperature of the inner core of the beam to stagnate a bit, and this can be observed after 15 minutes from the differences between the measured and predicted. This phenomenon can be seen clearly at 30 minutes, when the temperature measured and projected at 25 mm depth was wider than that reported at 15 minutes. The same occurs in subsequent intervals for depths of 50 mm and 100 mm (30, 45, and 60 minutes). The gap grew greater because the moisture was pushed to the top surface, and this movement of moisture to the upper portion of the beam eventually repressed the rise in temperature.

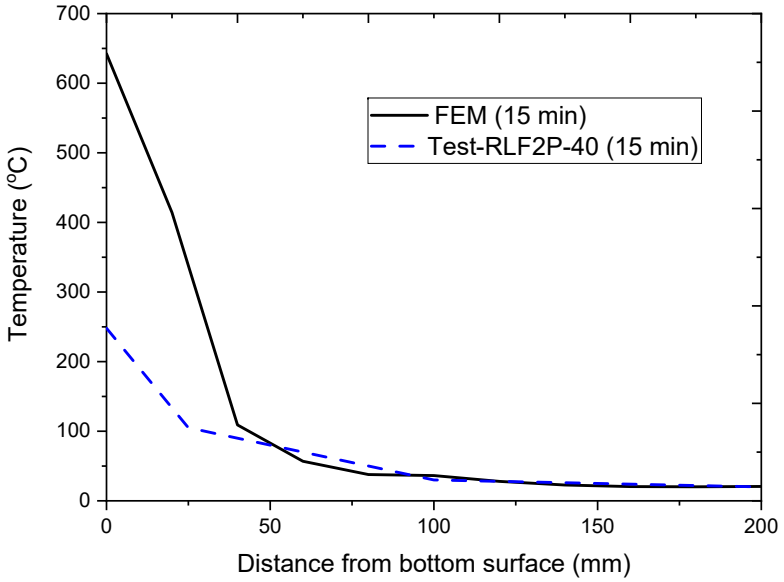

Figure 4.13: Temperature distribution across the depth at 15 minutes.

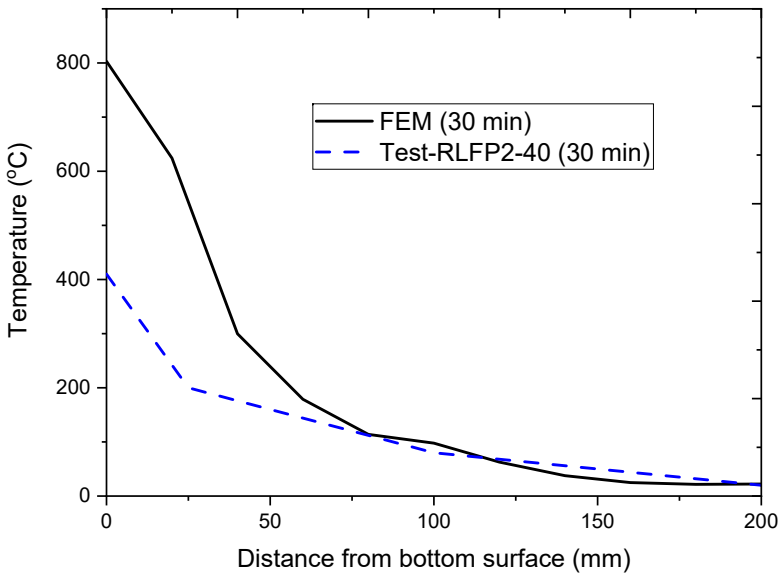

Figure 4.14: Temperature distribution across the depth at 30 minutes.

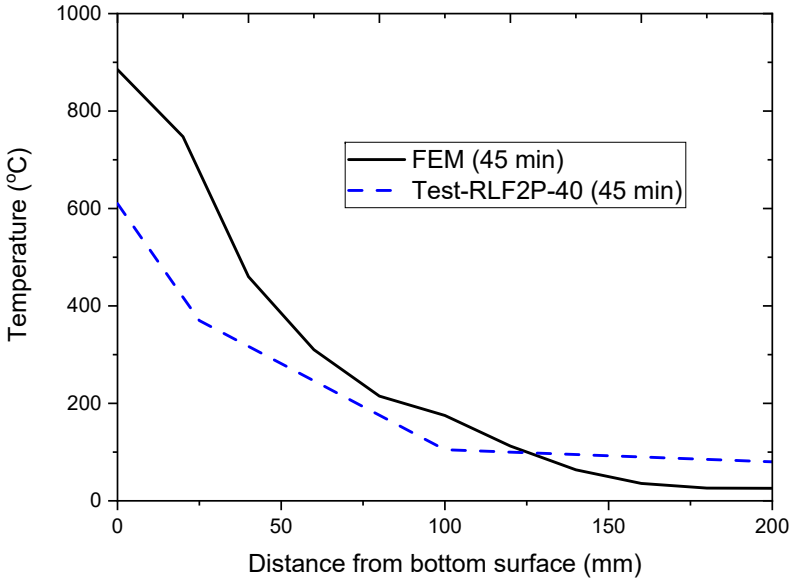

Figure 4.15: Temperature distribution across the depth at 45 minutes.

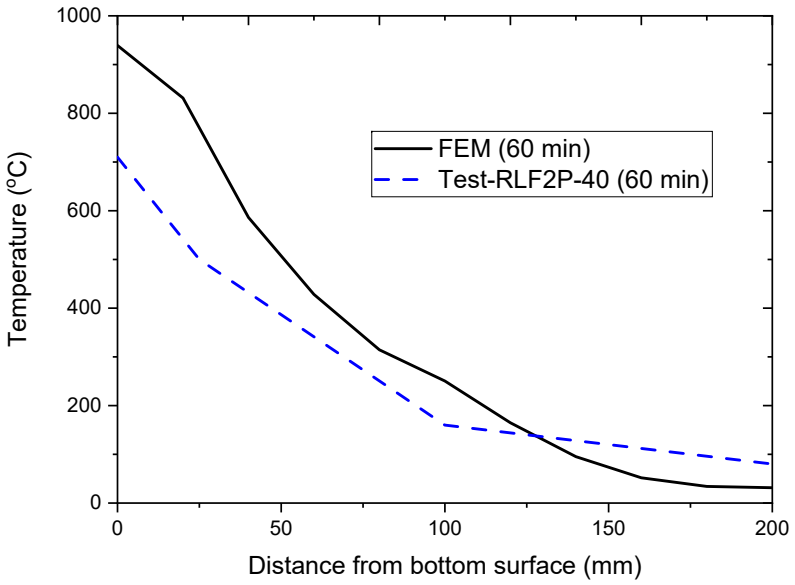

Figure 4.16: Temperature distribution across the depth at 60 minutes.

4.2.2.2 Model adequacy

In this section, the adequacy of the FEM model in predicting outcomes of the RLF2P-40 beam is investigated. A correlation analysis using linear regression was performed. A linear model was fit to scatter points of observed temperature against predicted temperature, at different 15, 30, 45, and 60 minutes. Scatter plots and the linear model fit to the scatter points are shown in Figures 4.17-4.20. It can be observed that the coefficient of determination (R^2) values are close to 1.0. This implies that the model is adequate enough to predict temperature distributions of the RLF2P-40 beam at different times and different distances from the bottom surface.

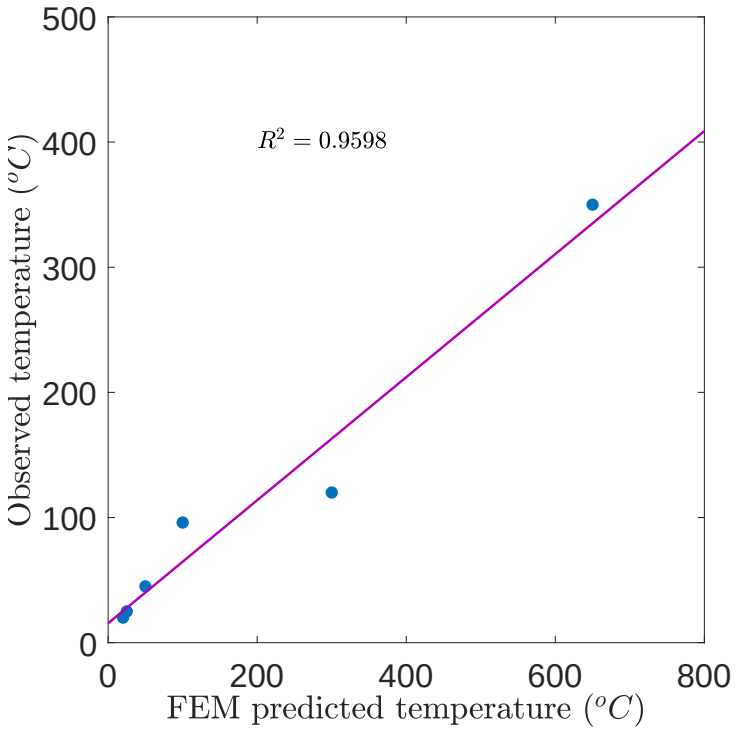

Figure 4.17: Scatter plot of observed temperatures of the RLF2P-40 against predicted temperatures at 15 minutes. A linear model is fit to the scatter points with $R^2 = 0.9598$

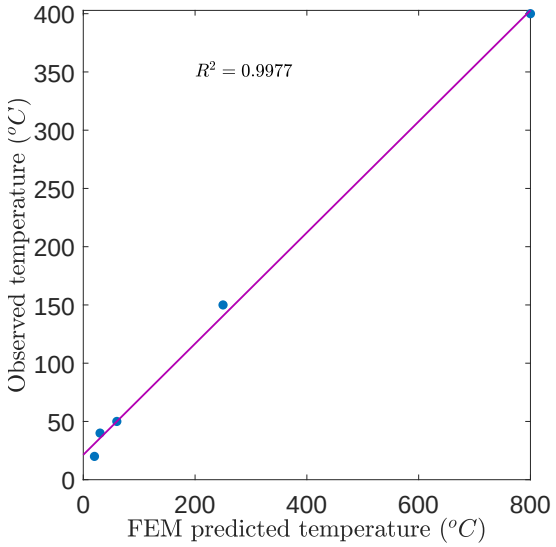

Figure 4.18: Scatter plot of observed temperatures of the RLF2P-40 against predicted temperatures at 30 minutes. A linear model is fit to the scatter points with $R^2 = 0.9977$

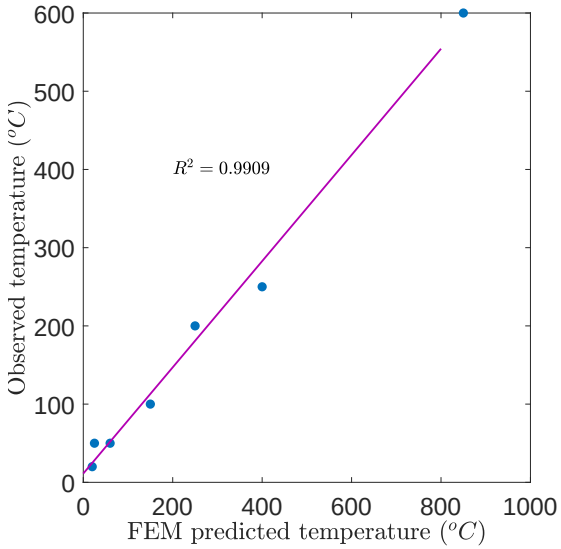

Figure 4.19: Scatter plot of observed temperatures of the RLF2P-40 against predicted temperatures at 45 minutes. A linear model is fit to the scatter points with $R^2 = 0.9909$

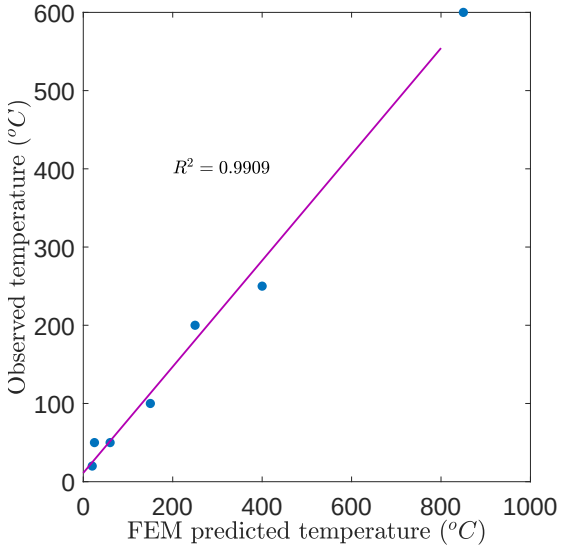

Figure 4.20: Scatter plot of observed temperatures of the RLF2P-40 against predicted temperatures at 60 minutes. A linear model is fit to the scatter points with $R^2 = 0.9896$

4.3 Structural analysis

This section presents the post-heat transfer structural analysis. The section presents one of the widely used structural response in fire resistance determination, namely: deflection history. Comparisons between experimental results from Kahanji (2016) and the predicted values are presented and discussed for three different categories grouped according to load ratios of 0.2, 0.4, and 0.6 corresponding to the applied midspan concentrated loads of 25kN, 50kN and 75kN, respectively on the beams as reported by Kahanji (2016).

4.3.1 Deflection History

4.3.1.1 Load ratio 0.2

In this category of test, Kahanji (2016) tested two beams (RLF2-2- and RLF4-20) in the furnance with an imposed load of 25kN applied at mid-span. As explained in Chapter 3, the results from the uncoupled heat transfer analysis were used to define the temperature field for the structural analysis phase and temperature dependent structural analysis was conducted with a pre-load of 25kN applied at mid-span. This procedure in ABAQUS is

called sequentially coupled thermal stress analysis.

The deflection evolution of the FEM model and the two experimental beams are given in Figure 4.21. The FEM model deflection is higher than the two experimental results for most parts of the 1-hour duration until the last 25 minutes. The robustness displayed by both beams is due to the existence of steel fibers not provided for in the model. The higher deflections by the two experimental beams in the last 25 minutes could be explained in terms of spalling which the FEM model did not account for. Kahanji (2016) reported spalling in these two beams which was characterised by loss of cross-section. This phenomenon decreased the local bending stiffness of the experimental beams, resulting in higher measured deflections than predicted by the FEM model. Despite the overestimation in the stiffness of the model and the lack of spalling modeling capabilities, the model predicted 60 minutes of no-failure performance.

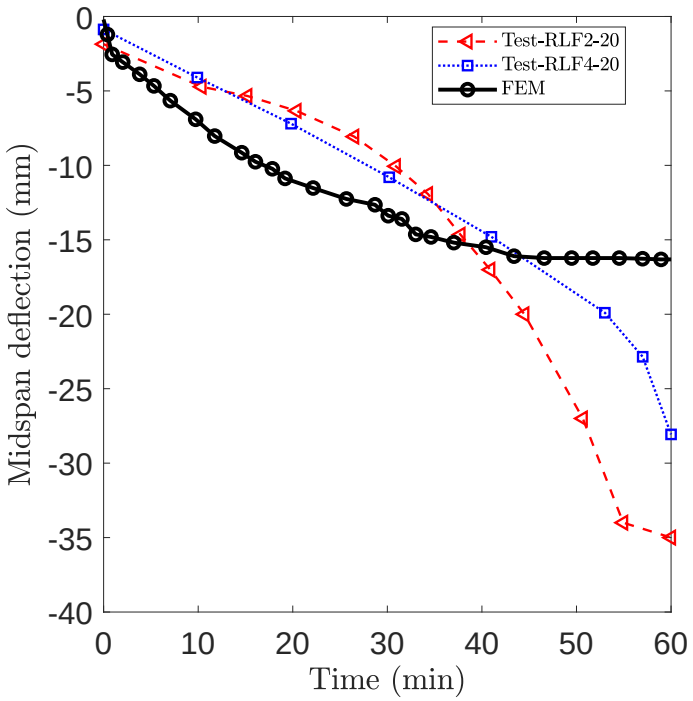

Figure 4.21: FEM versus experimental mid-span deflection for 0.2 load ratio.

4.3.1.2 Load ratio 0.4

The experimental mid-span deflection from the beams is compared under a load ratio of 0.4 in Figure 4.22, with the FEM model mid-span deflection. Just like in the 0.2

load ratio, the FEM model deflection data is higher than the one measured on the experimental beams until the last 20 minutes of the test. This can be explained by the failure of the FEM model to account for additional stiffness from fibres. The effect of fibres was not modelled in the ABAQUS FEM model. After the 40^{th} minute, the predicted deflection is lower than the deflection Kahanji (2016) measured on the experimental beam. This is due to the lack of the FEM model to capture the spalling phenomenon observed in the test by Kahanji (2016). The RLF2P-40 beam containing steel fibres did not undergo spalling and still recorded a lower deflection in comparison with the FEM model due to the higher stiffness in the beam as a results of steel fibres which were not accounted for in the FEM model.

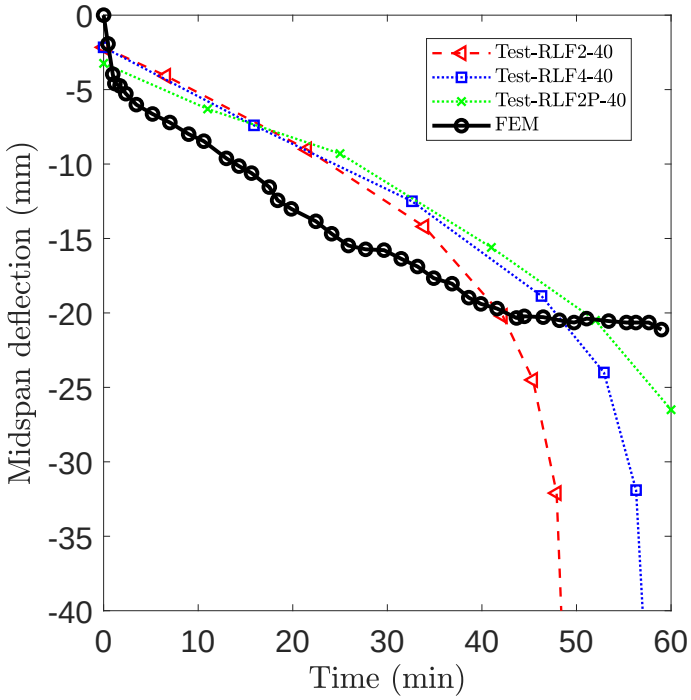

Figure 4.22: FEM versus experimental mid-span deflection for 0.4 load ratio.

4.3.1.3 Load ratio 0.6

The experimental mid-span deflection from the beams is compared under a load ratio of 0.6 in Figure 4.23, with the FEM model mid-span deflection. Just like in the 0.2 and 0.4 load ratio, the FEM model deflection data is higher than the one measured on the experimental beams until the last 10 minutes of the test. This can be explained by the

lack of steel fibre modelling capabilities in the ABAQUS FEM model to account for additional stiffness from fibres. After the 50^{th} minute the predicted deflection is lower than the deflection Kahanji (2016) measured on the experimental beam. This is due to the lack of the FEM model to capture the spalling phenomenon observed in the test by Kahanji (2016).

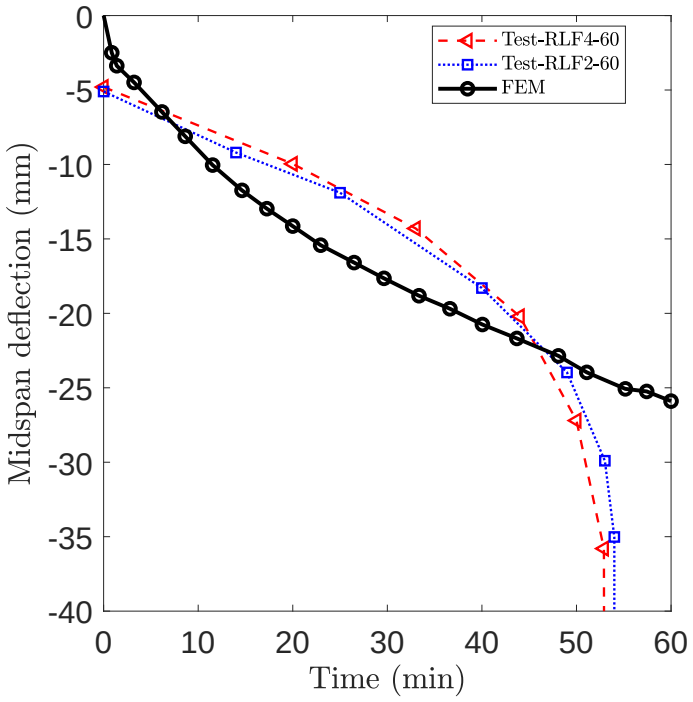

Figure 4.23: FEM versus experimental mid-span deflection for 0.6 load ratio.

4.4 Limitations of the model

Significant amounts of effort was made into the development of a numerical tool to be used for the investigation of fire resistance of UHPFRC beams. However, this model needs improvement as it has a number of deficiencies.

Firstly, the model did not account for effect of moisture content in the UHPFRC beams. Moisture content can be accounted for in ABAQUS by the values of specific heat capacity defined in the model. However, the values of specific heat capacity employed in the model were based on EN1992-1-2 equations which are based on HSC. These may differ from the values for UHPFRC.

Secondly, the model did not account for the influence of spalling in the beams. As reported by Kahanji (2016) spalling had a lot of influence on the fire resistance of UHPFRC beams. The author also mentioned that this phenomenon had a significant effect on the temperature distribution within the beams especially on areas close to the exposed surfaces and during the end of the test. Even though the author came across an approach of modelling spalling using temperature-pore pressure analysis available in ABAQUS, there was limited time and space to incorporate this information into this study. Modelling the effect of spalling mechanism is still a question for future research. The numerical tool developed here would be more suited to spalling-free concrete element like the beams that contained PP fibres.

Thirdly, despite modelling the tensile behaviour of UHPFRC as temperature dependent using ABAQUS's CPD model, the model did not explicitly incorporate the steel fibres since the UHPFRC matrix was modelled as plain concrete without steel fibres. The absence of steel fibres meant that the levels of ductility present in the test beams could not be fully realised in the FEM model. Ductility is one of the most important and valuable properties steel fibres induce in concrete. This can be seen from the deflection curves. The deflection curves of the test beams appear to be more ductile than those of the FEM model.

4.5 Fire resistance parametric study

This section presents a fire resistance parametric study using the developed FEM model. The FEM model has previously been used to investigate the thermal and mechanical response of UHPFRC beams subjected to the ISO834 fire curve and load levels of 0.2, 0.4 and 0.6 corresponding to point loads of 25, 50 and 75kN, respectively. The intent of this parametric study is to use the developed FEM model into investigating the fire resistance of UHPFRC beams by varying certain parameters. Two parameters are to be studied. The first parameter to be investigated in this parametric study is the hydrocarbon-fire-curve, which induces a different temperature distribution across the beam's cross-section. The second parameter, is the load ratio which is varied from 0.1 to 0.9 load ratios in steps of 0.1 load ratio. The thermal and mechanical response due to the ISO834 and hydrocarbon fire curve under load ratios from 0.1 to 0.9 were compared.

4.5.1 Parameters

As earlier discussed in Chapter 2, the fire resistance of an element is assessed in three different ways, that is, load bearing function, integrity, and insulation. When assessing the fire resistance of a beam, insulation is not a major concern but the load bearing and integrity functions are used.

The load bearing capacity is often assessed using deflection failure as limit state. In this case, the fire resistance of a beam is the time it takes until the beam exceeds a certain limiting deflection prescribed by prescriptive codes of practice.

On the other hand, the integrity function is assessed using temperature as limit state. In such a case, the element's load bearing capacity is assessed based on its fire penetration resistance. Two simplified procedures, notably, the 500^oC isotherm and the zone methods are used in prescriptive guidelines to compute the fire resistance of a member based on temperature as a limit state. Therefore, the parameters to be investigated in this fire resistance parametric study are:

1. Heating regime (temperature)

2. loading levels and resulting deflections.

4.5.2 Heating regime

Two heating regimes are investigated and compared, that is the ISO-834 and the hydrocarbon heating regimes. The temperature-time curve for the two heating regimes are presented in Figure 4.24. From the curves, it is clear that the hydrocarbon heating regime has a higher calorific value than the ISO 834. This implies that an element may undergo significant deformations and failure when subjected to a hydrocarbon fire than when subjected to a standard fire.

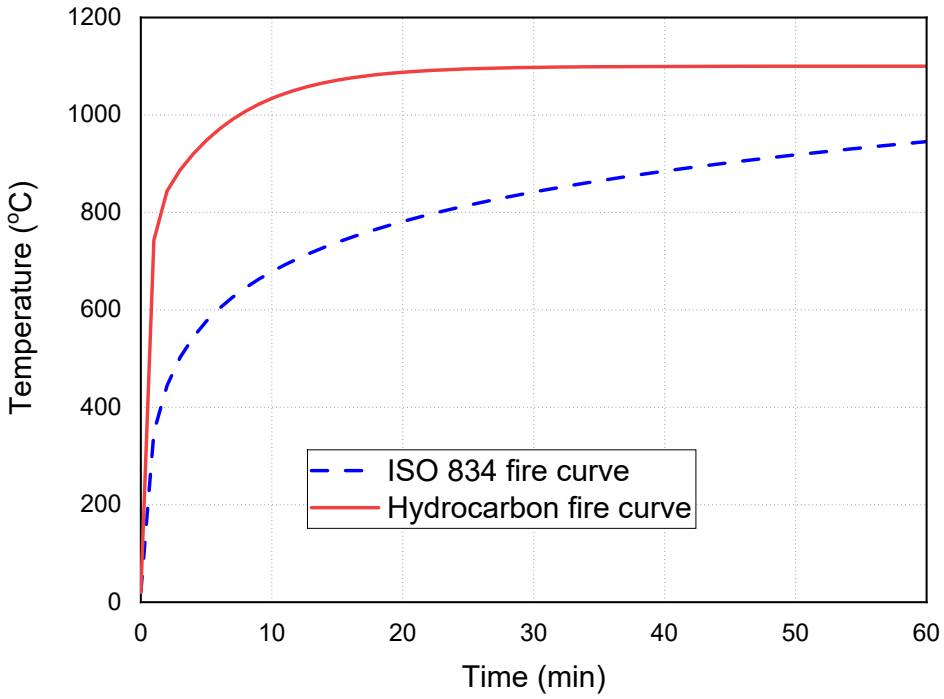

Figure 4.24: Temperature-time curves: Hydrocarbon versus ISO 834

4.5.2.1 Temperature distribution-Hydrocarbon curve

The temperature distribution simulated under the hydrocarbon heating regime is presented and discussed in this section. The simulated temperature distribution at selected depths across the mid-span of the beam over the 60 minutes duration of exposure to a

hydrocarbon fire curve is presented in Figure 4.25. The selected locations were bottom, top, 20, 60, 100 and 160mm from bottom. In comparison to the simulated temperatures by the ISO 834 curve (see Figure 4.3), the temperatures simulated by the hydrocarbon fire curve are higher which is in line with its higher calorific value. The results represent a response to fire of UHPFRC beams when used in bridges, petrochemical industry or tunnelling where fires with similar calorific value to the hydrocarbon curve is likely to occur. The next section delves into the comparisons of simulated temperature distribution at selected depths between the hydrocarbon and ISO 834 fire curve.

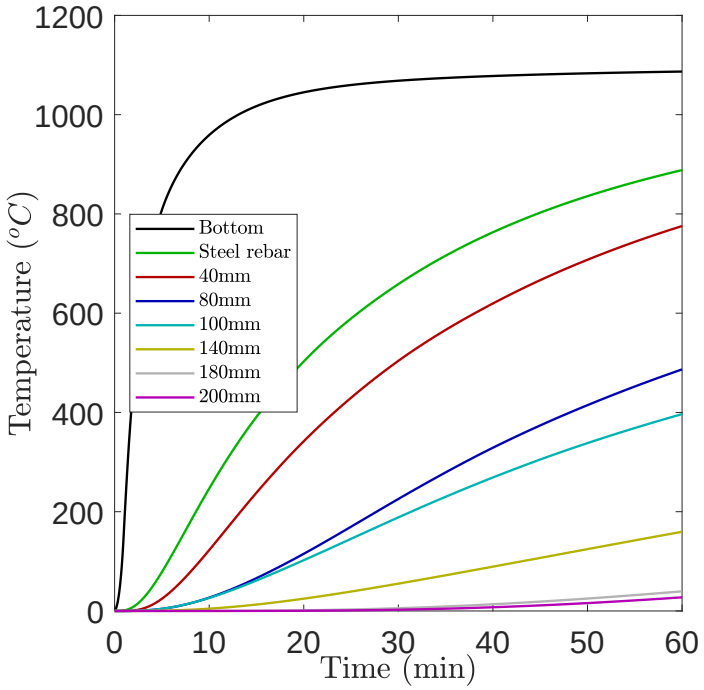

Figure 4.25: Temperature distribution through the cross-section of the beam from exposed surface due to the Hydrocarbon fire

4.5.2.2 Temperature development across the depth-HC vs. ISO 834

The generated temperature distributions from the hydrocarbon heating curve across the beam's 200 mm depth at selected time intervals are presented in Figure 4.26. The reported temperature values were recorded at the beam's midspan and located along the width centre. The corresponding temperature distribution across the entire thickness of the beam generated by the ISO 834 standard fire is presented in section 4.2.1 (see Figure 4.14).

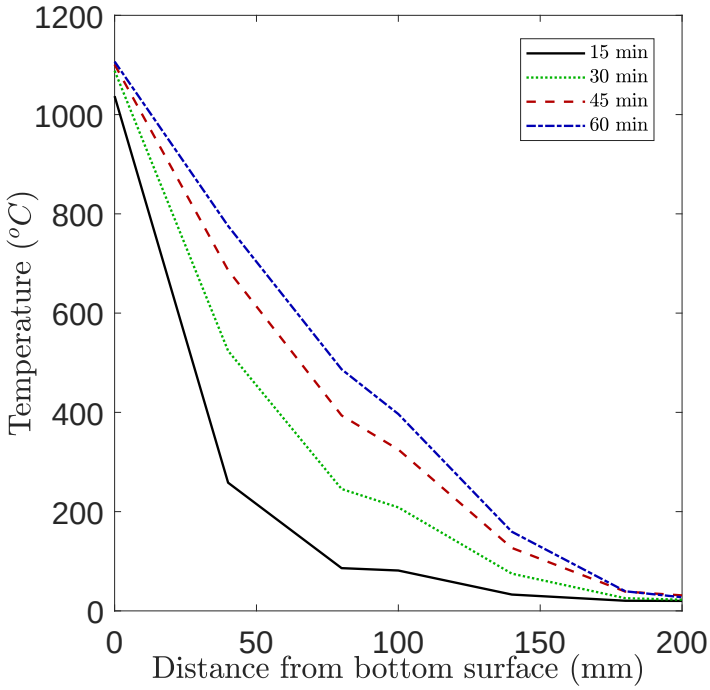

Figure 4.26: Temperature distribution across the beam's depth from exposed surface due to the Hydrocarbon fire

In Figures 4.27-4.30, the predicted temperature distributions from the exposed surface to the top surface, simulated from the ISO 834 standard fire and the hydrocarbon curve are compared. The temperature distributions were recorded at 15, 30, 45 and 60 minutes. As expected, due to its higher calorific value output, the predicted temperature response simulated from the hydrocarbon heating was higher than that generated from the standard fire curve. However, it can clearly be seen that the discrepancy between the two predicted temperature distribution gradually reduced with depth, matching each other at the unexposed top surface.

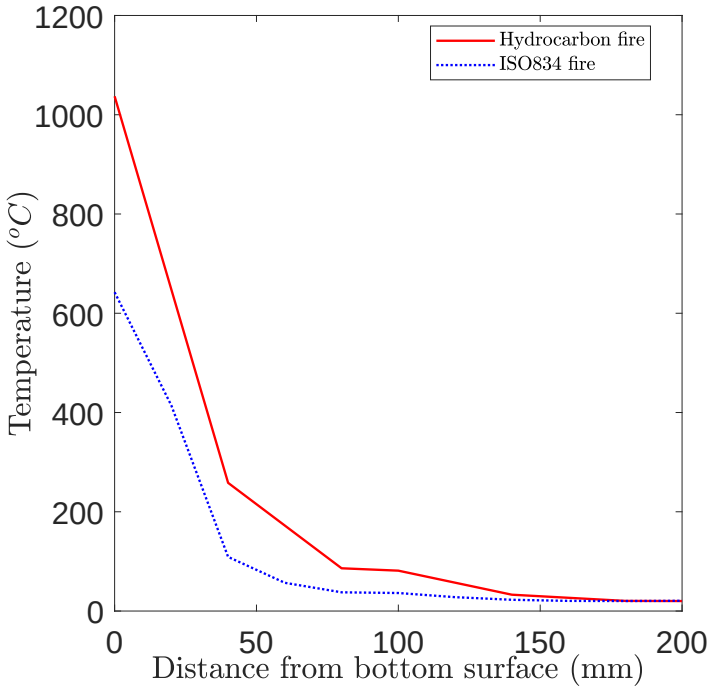

Figure 4.27: 15 minutes into the fire temperature development: ISO 834 versus Hydrocarbon

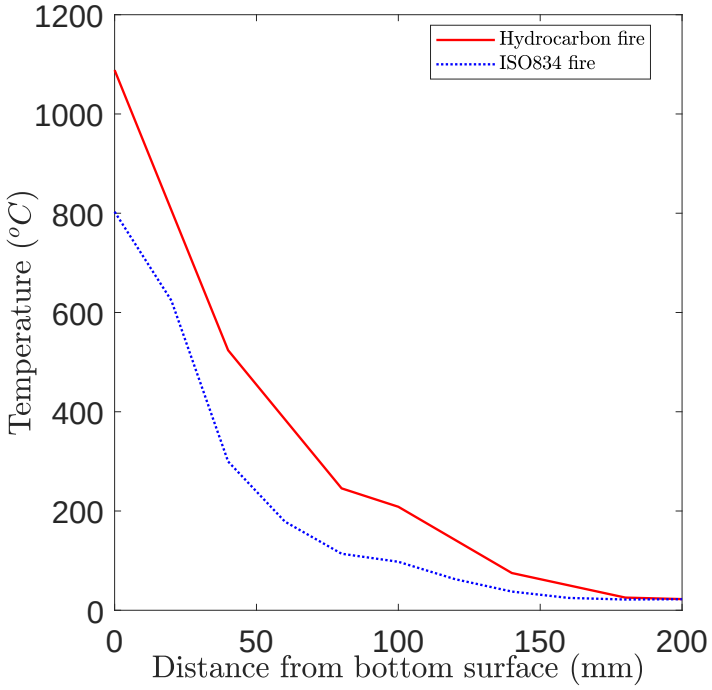

Figure 4.28: 30 minutes into the fire temperature development: ISO 834 versus Hydrocarbon

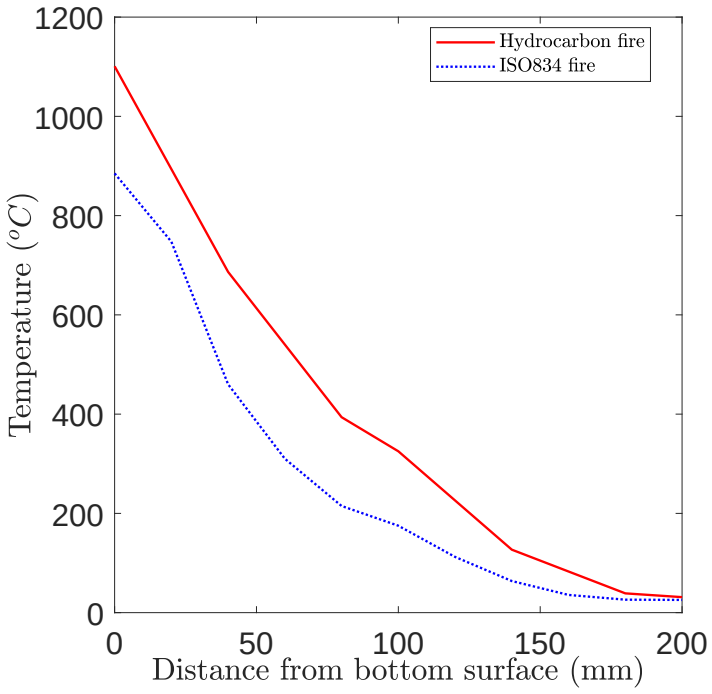

Figure 4.29: 45 minutes into the fire temperature development: ISO 834 versus Hydrocarbon

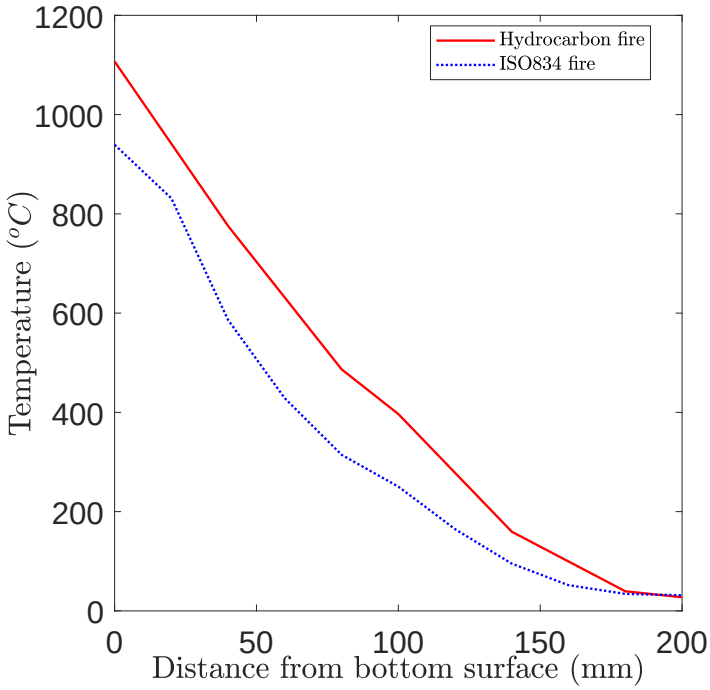

Figure 4.30: 60 minutes into the fire temperature development: ISO 834 versus Hydrocarbon

4.5.3 Load levels

In this section deflection failure under load levels from 0.1 to 0.9 load ratios are simulated and compared for the ISO 834 and hydrocarbon fire curves. The predicted failure times under the two heating regime are used to predict the fire resistance rating (FRR) of the beams. The predicted failure times and the FRR at each load ratio under both heating regimes are presented in Table 4.1. The failure was defined using the BS 1363 limiting deflection criteria ($L^2/400d$). For the beams considered in this parametric study, a value of 38.3mm was determined. As predicted, due to the high calorific value of the hydrocarbon fire curve, the deflection forecast under this temperature-time curve was higher for all nine load ratios. In the heat regime of ISO 834, failure was reported only at a load ratio of 0.7. However, the expected failure of hydrocarbon heating was reported at a much lower load ratio of 0.5 after approximately 55 minutes of exposure. Under the 0.6 load ratio, failure was reported in the hydrocarbon heating at 50 minutes, but no failure was reported in the normal heating. In both heating regimes, the failure rate was 0.7 at 35 and 50 minutes for the hydrocarbon and ISO 834 for the regular fire

curve, respectively.

In the load ratio group of 0.9, failure was recorded much earlier in both beams; at 11 minutes under the influence of a hydrocarbon fire and at 15 minutes under the exposure of a regular fire. It should be noted that the modeling did not take into account the spalling factor. The spalling phenomenon typically results in premature failure of the beams. The addition of PP fibres reduces the spalling effects and these modeling results will therefore reflect UHPFRC concrete beams containing PP fibres.

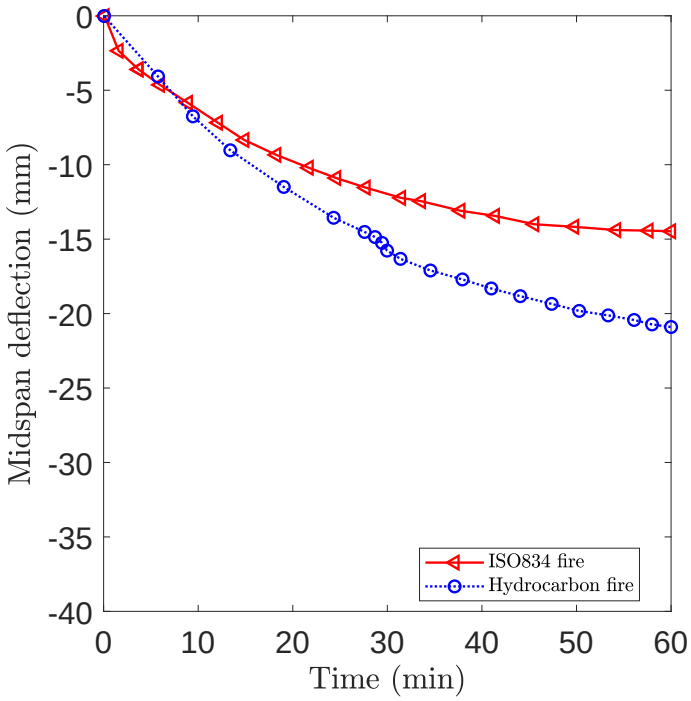

Figure 4.31: Hydrocarbon versus ISO 834 deflection response at 0.1 load ratio

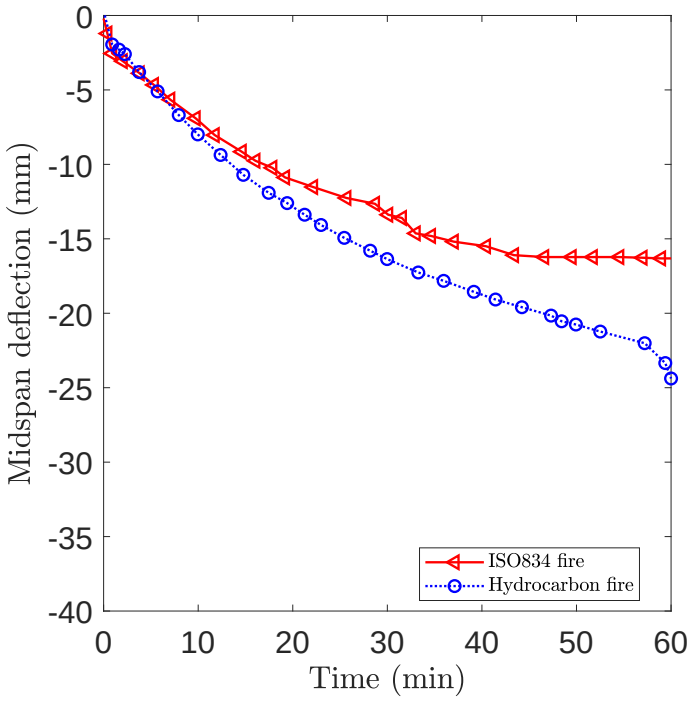

Figure 4.32: Hydrocarbon versus ISO 834 deflection response at 0.2 load ratio

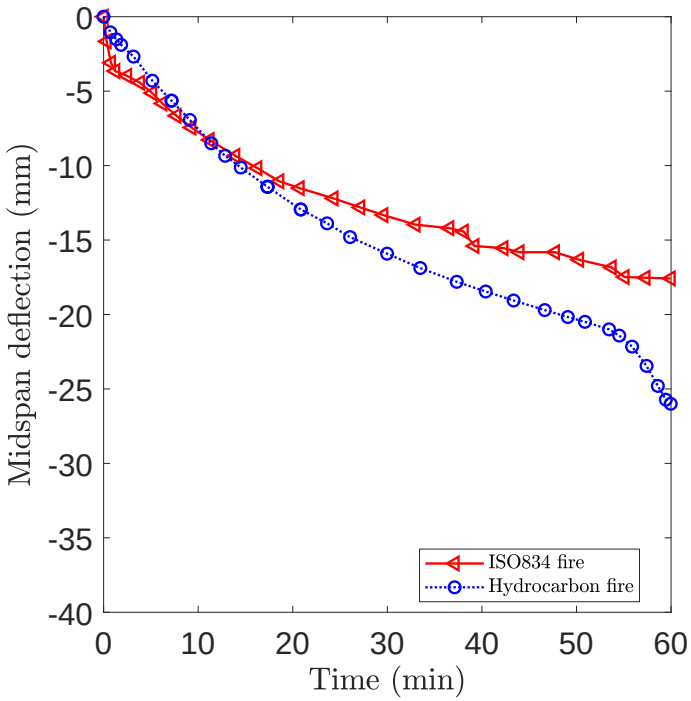

Figure 4.33: Hydrocarbon versus ISO 834 deflection response at 0.3 load ratio

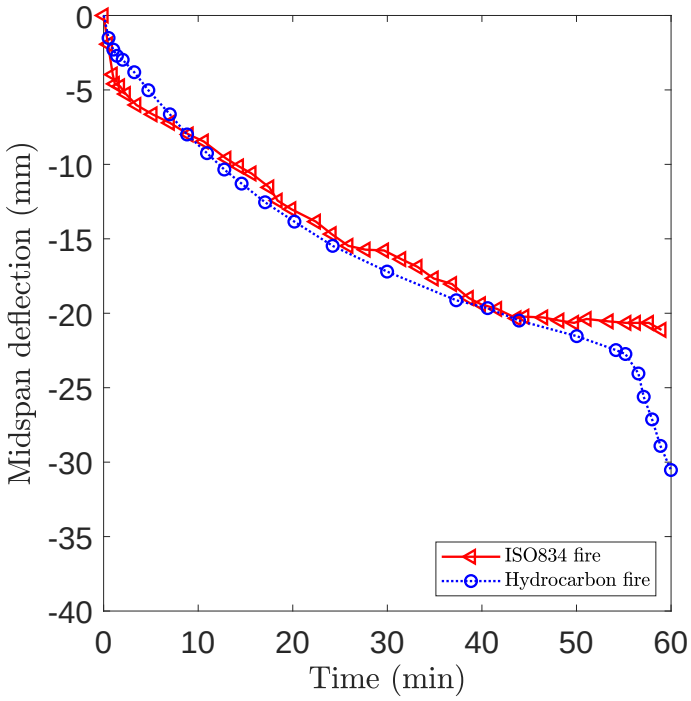

Figure 4.34: Hydrocarbon versus ISO 834 deflection response at 0.4 load ratio

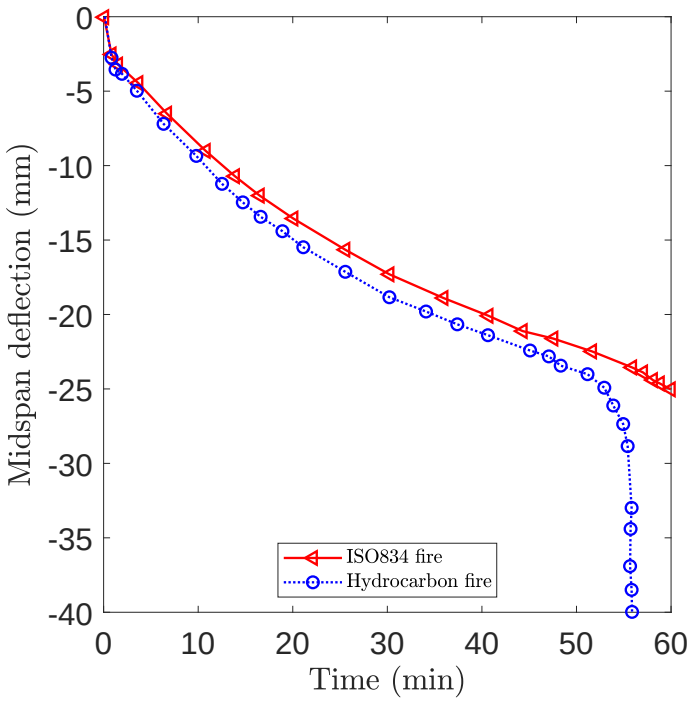

Figure 4.35: Hydrocarbon versus ISO 834 deflection response at 0.5 load ratio

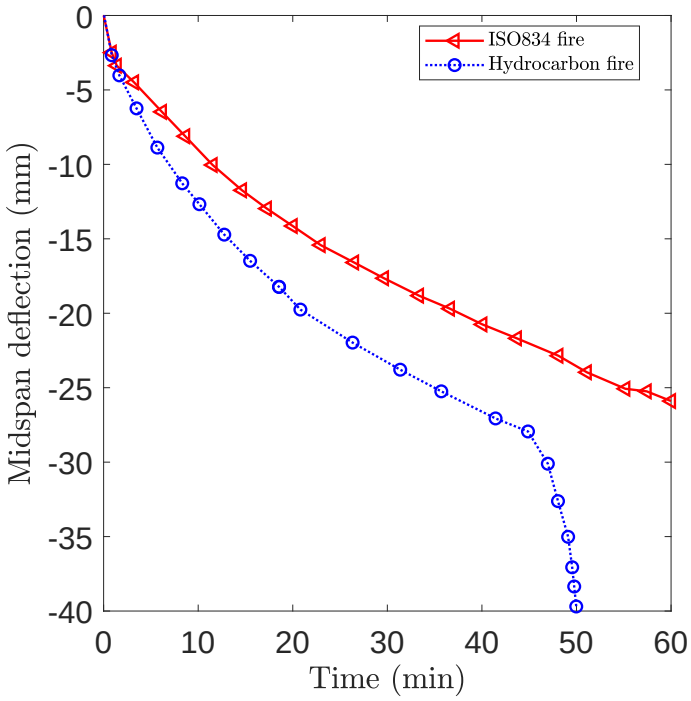

Figure 4.36: Hydrocarbon versus ISO 834 deflection response at 0.6 load ratio

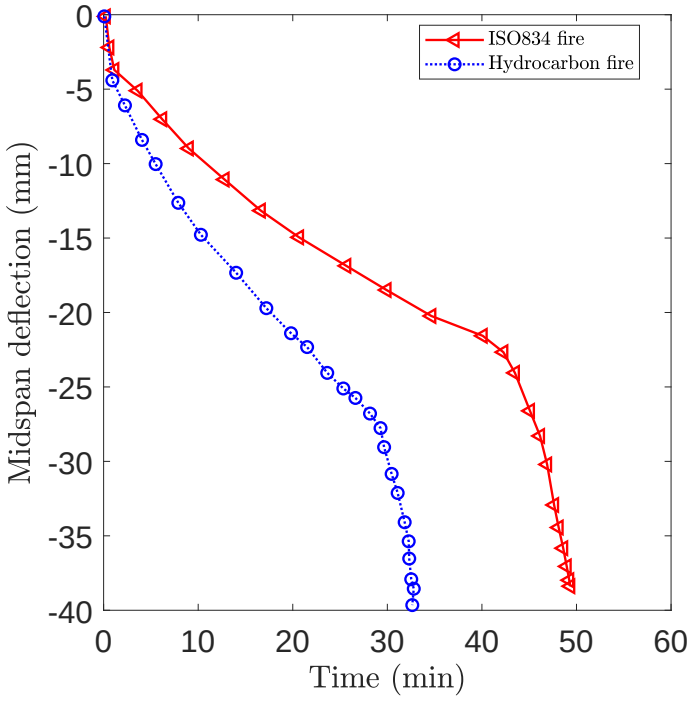

Figure 4.37: Hydrocarbon versus ISO 834 deflection response at 0.7 load ratio

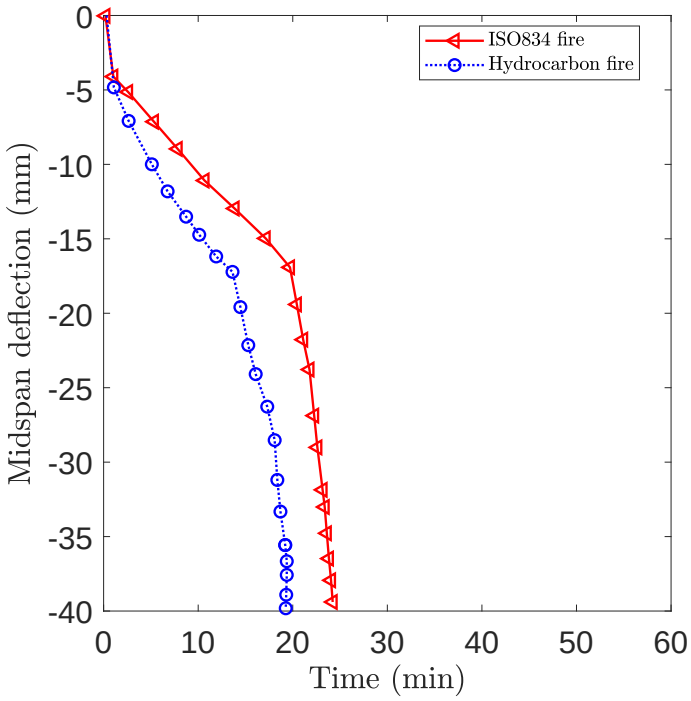

Figure 4.38: Hydrocarbon versus ISO 834 deflection response at 0.8 load ratio

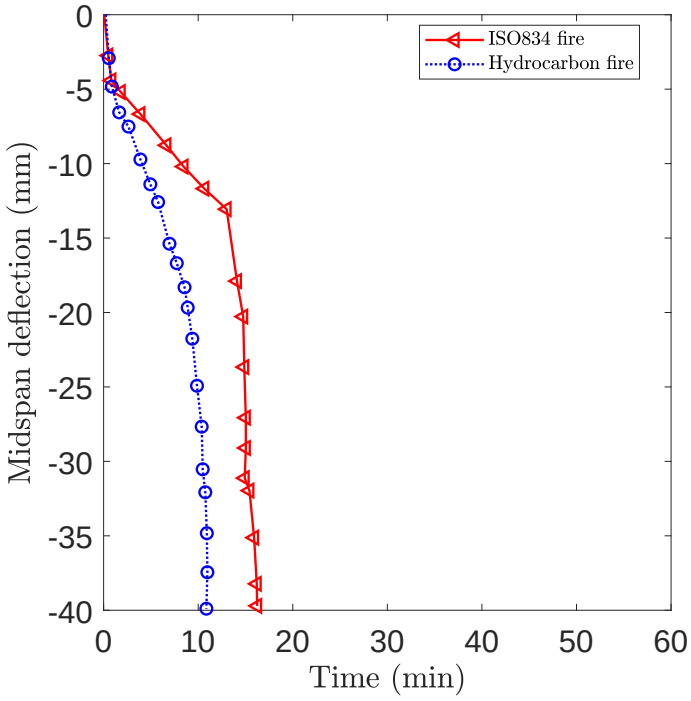

Figure 4.39: Hydrocarbon versus ISO 834 deflection response at 0.9 load ratio.

Table 4.1: Predicted failure times and fire resistances : ISO834 versus Hydrocarbon

	Failure time (min)		Fire resistance rating (min)	
Load ratio	ISO834	HC	ISO834	HC
0.1	-	-	60	60
0.2	-	-	60	60
0.3	-	-	60	60
0.4	-	-	60	60
0.5	-	55	60	30
0.6	-	48	60	30
0.7	50	35	30	30
0.8	23	19	0	0
0.9	15	11	0	0

4.6 Chapter overview

This chapter presented results that were observed during this study. The chapter also discusses the results. The chapter began by first comparing the predicted and experimental heat transfer response. The developed FEM model predict temperature distributions that were in agreement with experimental results. The predicted temperature distributions were then used to conduct a mechanical analysis and the predicted and measured response were compared and load ratios of 0.2, 0.4 and 0.6. The predicted deflection response was in good agreement with the measured deflection response. Despite being in close agreement with experimental data, the developed FEM models had their own limitations. These limitations were explained in terms of three characteristics, namely, moisture content, spalling mechanism and steel fibres. The FEM models were then used for a subsequent parametric analysis. Two parameters were considered, that is, heating regime and load ratio. Heating regime considered the ISO 834 and the hydrocarbon fire curve while the load ratios were varied from 0.1 to 0.9 in load ratio steps of 0.1. The fire resistance estimated using the parametric study can be used for estimation of fire performance in spalling-free UHPFRC beams.

Chapter 5

CONCLUSIONS AND RECOMMENDATIONS

5.1 Conclusions

From the literature review and to the best knowledge of the author, research into the development of finite element models that predicts the fire resistance of UHPFRC beams exposed to fire is very scarce. This may be as a results of UHPFRC technology being a new subject. This study has presented a finite element model that reasonably predicts the thermal and mechanical response of UHPFRC beams when subjected to elevated temperatures. The model was validated against experimental results obtained by Kahanji (2016). With respect to the developed FEM model, two important conclusions can be made:

- The model reasonably predicts the temperature distribution. It must be noted, however, that the model did not account for the effect of moisture content, spalling and polypropylene fibres on the temperature distribution.
- The model reasonably predicts the defection history under the load ratios of 0.2, 0.4 and 0.6. It must be noted, however, that the model did not account for the effect of spalling and steel fibres on the deformation history.

The developed FEM models were then used for subsequent parametric study. The objective of the parametric study was to investigate the fire resistance of the UHPFRC

under the characterisation of heating regimes and a broad scope of load ratios. The ISO834 and the hydrocarbon heating regimes were considered and compared. Load rations from 0.1 to 0.9 under both the ISO834 and the hydrocarbon heating regimes were investigated. With respect to the conducted parametric study, the following conclusions can be drawn:

- The temperature distributions predicted from the hydrocarbon heating regimes were higher than those predicted from the ISO834 heating regime. This was attributed to the higher calorific value of the hydrocarbon fire curve when compared to that of the ISO834 curve.
- The deflections resulting from the hydrocarbon fire curve were higher than the deflections resulting from the ISO834 heating regime. As a results, in some cases, the hydrocarbon fire resistance ratings were 30 minutes lower than the ratings determined using the ISO834 fire. Failure of the beams under the ISO834 curve was observed when the load ratio exceeded 0.6 while under the hydrocarbon curve failure was observed at much lower load ratio exceeding 0.4.

The results obtained from the parametric study could be useful in the estimation of fire resistance of UHPFRC members which are spalling resistant, especially, those containing polypropylene fibres. However, attention should be given to the application of these fire resistance values. The fire resistance values predicted by the ISO 834 curve are more applicable to building fires but those predicted by the hydrocarbon fire curve are more applicable to bridge and petrochemical industry types of fire.

5.2 Research contribution

Current structural fire design advocates for performance based-design as the most robust and rational tool for fire resistance assessment of structural elements. However, the experimental approach to performance-based design is very expensive. With the advancement in numerical and computer simulations, versatile finite element software packages like ABAQUS could serve a useful purpose for developing numerical tools for conducting inexpensive performance fire design. In as much as such tools are

readily available for conventional concrete, they are very scarce for UHPFRC. The main research contribution in this dissertation is the development of reasonably accurate FEM models of UHPFRC beams exposed to fire and utilising such a tool in a fire resistance parametric study.

5.3 Challenges

Despite tremendous effort made in developing the FEM models, the author faced a number of challenges, which include among others:

- Difficulty in modelling the influence of moisture content in the UHPFRC beams. Moisture content has a significant influence on the temperature development of an element exposed to fire.
- Difficulty in modelling the influence of spalling when UHPFRC beams are subjected to fire. The spalling mechanism has an influence on the temperature distribution and deflection response. The author only discovered at the end of this study that an attempt could be made to model spalling mechanism in ABAQUS using the temperature-pore pressure analysis.
- Challenges in modelling the effect of steel fibres contained in real UHPFRC beams. This has an influence of the stiffness and ductility of UHPFRC beams.

5.4 Recommendations

With the challenges highlighted in the previous section, the author makes the following recommendations for future work:

- Research work should be directed towards the development of both analytical and numerical models that account for the influence of moisture content in UHPFRC beams.
- Research work into the numerical modelling of fire spalling mechanism in UHPFRC using a finite element approach would be ground-breaking. Analytical models would also be very useful and easy to apply by a lay engineer.
- Research work into the numerical modelling of the UHPFRC beams with steel fibres embedded in them at a macroscopic level would help in developing models with realistic predictions.

REFERENCES

ABAQUS (2018), *ABAQUS/Standard User's Manual, Version 6.9*, Dassault Systèmes Simulia Corp, United States.

ACI/TMS Committee 216 (1997), 'ACI 216.1-97 / TMS 0216.1-97: Standard Method for Determining Fire Resistance of Concrete and Masonry Construction Assemblies'.

AFGC (2013), 'Documents scientifiques et techniques Bétons fibrés à ultra-hautes performances Ultra High Performance Fibre-Reinforced Concretes Recommendations', *Recommandations provisoires.Janvier* .

American Concrete Institute (2018), 'CT-18: ACI Concrete Terminology', *Topics in Concrete* .

Ariyanayagam, A. D. and Mahendran, M. (2013), 'Fire safety of buildings based on realistic fire time-temperature curves', *Proceedings of the 19th International CIB World Building Congress, Brisbane 2013: Construction and Society* pp. 1–13.
URL: *http://eprints.qut.edu.au/61929/*

ASTM E119-20 (2020), *Standard test methods for fire test of building construction and materials*.
URL: *http://www.astm.org*

Babrauskas, V. (2016), 'Book review: Temperature Calculation in Fire Safety Engineering', *Journal of Fire Sciences* **34**(6), 530–533.
URL: *http://doi.org/10.1177/0734904116664535*

Bachman, R., Champion, L., Goodyear, D., Griffis, L., Herrmann, A. and Mcallister, T. (2018), 'Advocating for Performance-Based Design Report to the Structural Engineering Institute Board of Governors', *Structural Egnineering Institute - ASCE* .

Bahr, O., Schaumann, P., Bollen, B. and Bracke, J. (2013), 'Young's modulus and Poisson's ratio of concrete at high temperatures: Experimental investigations', *Materials and Design* **45**, 421–429.
URL: *http://doi.org/10.1016/j.matdes.2012.07.070*

Banerji, S., Kodur, V. and Solhmirzaei, R. (2020), 'Experimental behavior of ultra high performance fiber reinforced concrete beams under fire conditions', *Engineering Structures* **208**, 110316.
URL: *http://doi.org/10.1016/j.engstruct.2020.110316*

Benjamin A., G. (2006), 'Material Property Characterization of Ultra-High Performance Concrete', *FHWA* .

Bernardi, S., Jacomo, D. and Boudry, F. (2016), Overlay Ductal®: a durable solution for bridges retrofitting, *in* 'First International Interactive Symposium on UHPC'.
URL: *http://doi.org/10.21838/uhpc.2016.119*

Brushlinsky, N., Ahrens, M., Sokolove, S. and Wagner, P. (2017), 'World Fire Statistics. Bulletin N^{o}22', *World Fire Statistics* p. 56.
URL: *https://www.ctif.org/sites/default/files/ctif*$_{r}$*eport*22$_{w}$*orld*$_{f}$*ire*$_{s}$*tatistics*$_{2}$017.*pdf*

BS 476-22 (1987), 'Fire tests on building materials and structures', *British Standards Institution* .

Buchanan, A. and Abu, A. (2017), *Structural Design For Fire Safety*, 2nd edition edn, John Wiley Sons Ltd, New Zealand.

Capua, D. D. and Mari, A. R. (2007), 'Nonlinear analysis of reinforced concrete cross-sections exposed to fire', *Fire Safety Journal* **42**(2), 139–149.
URL: *http://doi.org/10.1016/j.firesaf.2006.08.009*

Castillo, C. and Durrani, A. J. (1990), 'Effect of transient high temperture on high-strength concrete', *ACI Materials Journal* **87**(1), 47–53.

Chung, J. H., Consolazio, G. R. and McVay, M. C. (2006), 'Finite element stress analysis of a reinforced high-strength concrete column in severe fires', *Computers and Structures* **84**(21), 1338–1352.
URL: *http://doi.org/10.1016/j.compstruc.2006.03.007*

CTIF (2019), 'World Fire Statistics'.
URL: *https://www.ctif.org/world-fire-statistics*

Dai, J. G., Gao, W. Y. and Teng, J. G. (2015), 'Finite element modeling of insulated FRP-strengthened RC beams exposed to fire', *Journal of Composites for Construction* **19**(2).
URL: *http://doi.org/10.1061/(ASCE)CC.1943-5614.0000509*

Ellingwood, B. and Lin, T. D. (1991), 'Flexure and shear behavior of concrete beams during fires', *Journal of Structural Engineering (ASCE)* **117**.
URL: *http://10.1061/(ASCE)0733-9445(1991)117:2(440)*

EN 1992-1-2 (2008), 'Eurocode 2: Design of concrete structures - Part 1-2: General rules. Structural fire design', *British Standards Institution* .

EN 1992-2 (2005), 'Eurocode 2: Design of concrete structures - Part 2: Concrete bridges - Design and detailing rules', *British Standards Institution* . .

EN 1993 (2005), EN 1993-1-2: Design of steel structures - Part 1-2: General rules - Structural fire design, Technical report.

Firmo, J., Arruda, M. and Correia, J. (2015), 'Numerical simulation of the fire behaviour of thermally insulated reinforced concrete beams strengthened with EBR-CFRP strips', *Composite Structures* **126**(11), 360–370.
URL: *https://doi.org/10.1016/j.compstruct.2015.02.084*

Franssen, J.-M. and Real, P. V. (2016), *Fire design of steel structures Eurocode*, European Convention for Constructional Steelwork.
URL: *https://onlinelibrary.wiley.com/doi/book/10.1002/9783433607008*

Gao, W. Y., Dai, J. G., Teng, J. G. and Chen, G. M. (2013), 'Finite element modeling of reinforced concrete beams exposed to fire', *Engineering Structures* **52**(July), 488–

501.
URL: *https://doi.org/10.1016/j.engstruct.2013.03.017*

Graybeal, B. A. (2007), 'Compressive behavior of ultra-high-performance fiber-reinforced concrete', *ACI Materials Journal* **104**(2), 146–152.
URL: *https://doi.org/10.14359/18577*

Guerrini, G. L. (2000), 'Applications of high-performance fiber-reinforced cement-based composites', *Applied Composite Materials* **7**(May), 195–207.

Habel, K., Viviani, M., Denarié, E. and Brühwiler, E. (2006), 'Development of the mechanical properties of an Ultra-High Performance Fiber Reinforced Concrete (UHPFRC)', *Cement and Concrete Research* **36**(7), 1362–1370.
URL: *https://doi.org/10.1016/j.cemconres.2006.03.009*

Huang, Z. and Platten, A. (1997), 'Nonlinear Finite Element Analysis of Planar Reinforced Concrete Members Subjected to Fires', *ACI Structural Journal* **94**(3), 272–281.
URL: *https://doi.org/10.14359/479*

Hurley, M. J. and Rosenbaum, E. R. (2019), *Performance-based fire safety design*, 1st edn, Taylor Francis Limited, United States.

ISO 834-1 (1999), 'Fire-resistance tests - Elements of building construction - Part 1: General requirements', *ISO Standard* .

Japan Society of Civil Engineers (2008), 'Recommendations for Design and Construction of High Performance Fiber Reinforced Cement Composites with Multiple Fine Cracks (HPFRCC)', *Concrete Engineering Series* .

Kahanji, C. (2016), Fire Perfomance of Ultra-High Perfomance Fibre Reinforced Concrete Beams, PhD thesis, Ulster University.

Kahanji, C., Ali, F. and Nadjai, A. (2016), 'Explosive spalling of ultra-high performance fibre reinforced concrete beams under fire', *Journal of Structural Fire Engineering* **7**(4), 328–348.

Kahanji, C., Ali, F., Nadjai, A. and Alam, N. (2018), 'Effect of curing temperature on the behaviour of UHPFRC at elevated temperatures', *Construction and Building Materials* **182**(September), 670–681.
URL: *https://doi.org/10.1016/j.conbuildmat.2018.06.163*

Kallada, J. and Hostikka, S. (2019), 'Predictive Computational Fluid Dynamics Simulation of Fire Spread on Wood Cribs', *Fire Technology* **55**(6), 2245–2268.
URL: *https://doi.org/10.1007/s10694-019-00855-3*

Kodur, V. (2014), 'Properties of concrete at elevated temperatures', *International Scholarly Research Notices Civil Engineering* **2014**(468510), 15 pages.
URL: *https://doi.org/10.1155/2014/468510*

Kodur, V. K. and Dwaikat, M. (2008), 'A numerical model for predicting the fire resistance of reinforced concrete beams', *Cement and Concrete Composites* .
URL: *https://doi.org/10.1016/j.cemconcomp.2007.08.012*

Kodur, V. K., Dwaikat, M. M. and Dwaikat, M. B. (2008), 'High-temperature properties of concrete for fire resistance modeling of structures', *ACI Materials Journal* **105**(5), 517–527.
URL: *https://doi.org/10.14359/19982*

Lakhani, H., Kamath, P., Bhargava, P., Singh, T. and Reddy, G. R. (2013), 'Simulation of fire resistance of reinforced concrete structural members', *Journal of Structural Engineering (India)* **40**(1), 7–11.

Liang, X. (2018), Experimental Study of UHPC with High Fire Resistance and Meso-Scale Modelling, Master's thesis, University of Technology Sydney.

Mago, N., Hicks, S. and Simms, W. I. (2014), Sequentially coupled thermal-stress analysis of a new steel- concrete composite slab under fire, *in* '2014 SIMULIA Customer Conference', Vol. 29, p. 37.
URL: *https://doi.org/10.13140/RG.2.2.26406.93763*

Mai, V. C., Nguyen, T. C. and Dao, C. B. (2020), 'Numerical simulation of ultra-high-performance fiber-reinforced concrete frame structure under fire action', *Asian*

Journal of Civil Engineering **21**(5), 797–804.
URL: *https://doi.org/10.1007/s42107-020-00240-4*

Naaman, A. E. (2003), 'Engineered Steel Fibers with Optimal Properties for Reinforcement of Cement Composites', *Journal of Advanced Concrete Technology* **1**(3), 241–252.
URL: *https://doi.org/10.3151/jact.1.241*

Naaman, A. E. (2009), 'High Performance Fiber Reinforced Cement Composites: Classification and Applications', *CBM-CI International Workshop, Karachi, Pakistan* pp. 389–401.
URL: *https://doi.org/978-969-8620-06-6*

Neville, A. (2012), *Properties of Concrete - 5th Edition*, Pearson Education Limited, The University of California.

Park, S. H., Kim, D. J., Ryu, G. S. and Koh, K. T. (2012), 'Tensile behavior of ultra high performance hybrid fiber reinforced concrete', *Cement and Concrete Composites* **34**(2), 172–184.
URL: *https://doi.org/10.1016/j.cemconcomp.2011.09.009*

Parkinson, D. L., Kodur, V. and Sullivan, P. D. (2008), *Performance-Based Design of Structural Steel for Fire Conditions*, American Society of Civil Engineers.
URL: *https://ascelibrary.org/doi/abs/10.1061/9780784409633*

Phan, L. (1996), *Fire Performance of High-Strength Concrete: A Report of the State-of-the-Art*, National Institute of Standards and Technology, Gaithersburg.

Purkiss, J. A. and Li, L. Y. (2013), *Fire safety engineering design of structures, Third edition*, Taylor & Francis.
URL: *https://doi.org/10.1201/b16059*

Shafiifar, M., Farzad, M. and Azizinamini, A. (2017), 'Experimental and numerical study on mechanical properties of Ultra High Performance Concrete (UHPC)', *Construction and Building Materials* **156**(December), 402–411.

Shi, C., Wu, Z., Xiao, J., Wang, D., Huang, Z. and Fang, Z. (2015), 'A review on ultra high performance concrete: Part I. Raw materials and mixture design', *Construction*

and Building Materials **101**(December), 741–751.
URL: *https://doi.org/10.1016/j.conbuildmat.2015.10.088*

Wille, K., El-Tawil, S. and Naaman, A. E. (2014), 'Properties of strain hardening ultra high performance fiber reinforced concrete (UHP-FRC) under direct tensile loading', *Cement and Concrete Composites* **48**(April), 53–66.
URL: *https://doi.org/10.1016/j.cemconcomp.2013.12.015*

Wille, K., Naaman, A. and El-Tawll, S. (2011), 'Optimizing Ultra-High-Performance Fiber-Reinforced Concrete', *Concrete International* **33**(9), 35–41.